CONFIDENTIAL

FP7-ICT Future Networks
SPECIFIC TARGETTED RESEARCH PROJECT
Project Deliverable

PHYDYAS Doc. Number	PHYDYAS_ 002
Project Number	ICT - 211887
Project Acronym+Title	PHYDYAS – PHYsical layer for DYnamic AccesS and cognitive radio
Deliverable Nature	Report
Deliverable Number	D2.1
Contractual Delivery Date	July 1st, 2008
Actual Delivery Date	July 22, 2008
Title of Deliverable	Data-aided synchronization and initialization (single antenna)
Contributing Workpackage	WP2
Project starting date; Duration	01/01/2008; 30 months
Dissemination Level	CO
Author(s)	Mario Tanda and Tilde Fusco (UNINA – WP2 leader), Markku Renfors (TUT), Jérôme Louveaux (UCL), Maurice Bellanger (CNAM)

Abstract: After introducing the FBMC concept, the reference prototype filter is described. The filter parameters, particularly the impulse response, are crucial for the initialization of the system. Then, data aided techniques are presented for the full block scheme (downlink) and for groups of sub-channels (uplink). Methods to estimate the carrier frequency offset and the symbol timing offset are described. Finally, in order to accelerate the process, transmission burst shaping and filter bank memory preloading are investigated. Performance evaluation has been carried out in most cases. Attention has been paid to the issue of compatibility with OFDM.
The next step will be the integration of a simulation software and its delivery to WP9 for implementation in the demonstrator and evaluation.

Contents

Notations

$\angle\{x\}$ the argument of a complex number x in $[0,2\pi)$,

$\mathrm{Re}\{.\}$ real part

$\mathrm{Im}\{.\}$ imaginary part

$(.)^*$ complex conjugation

$|.|$ absolute value

M overall number of subcarriers, FFT size

M_u^i number of used subcarriers of the ith user (in single-user case, index i is dropped)

M_u^i set of used subcarriers of the ith user

M_v number of virtual (unused) subcarriers

K overlapping factor in prototype filter design

α roll-off factor in prototype filter design

L prototype filter length

T_s sampling interval (at SFB output and AFB input)

f_s sampling rate (at SFB output and AFB input)

T OQAM symbol duration; $T=MT_s$

Δf subcarrier spacing, $\Delta f=1/T=f_s/M$

k subcarrier index (k=0, …, M-1; k=0 corresponds to center subcarrier)

n time index at subcarrier rate

m time index at SFB output/AFB input

i user index in multiuser cases

U number of users

$v^R(n)$ real part of (arbitrary) complex sequence $v(n)$

$v^I(n)$ imaginary part of (arbitrary) complex sequence $v(n)$

$p(t)$ prototype filter impulse response, continuous-time model

$p(m)$ prototype filter impulse response, discrete-time [(1)]

$$p(m)=\sqrt{T_s}\,p\left(mT_s\right)$$

$P(z)$ prototype filter transfer function

$f_k(m)$ analysis filter impulse response for subchannel k

$F_k(z)$ analysis filter transfer function for subchannel k

$G_k(z)$ synthesis filter transfer function for subchannel k

$g_k(m)$ synthesis filter impulse response for subchannel k

$$g_k(m)=p\left(m\right)e^{j\frac{2\pi}{M}k\left(m-\frac{L-1}{2}\right)}$$

$p_{k,n}(m)$ SFB impulse response for real symbol $d_{k,n}$ (see also definition of $s(m)$)

$$p_{k,n}(m)=\theta_{k,n}g_k\left(m-nM/2\right)$$

$$=\theta_{k,n}\beta_{k,n}p\left(m-nM/2\right)e^{j\frac{2\pi}{M}km}$$

$\theta_{k,n}$ phase mapping between real data sequence and complex samples at the SFB input

In general,

$$\theta_{k,n} = \begin{cases} \pm 1 & \text{for } k+n \text{ even} \\ \pm j & \text{for } k+n \text{ odd} \end{cases}$$

The recommended choice (following Siohan's papers) is[2]:

$$\theta_{k,n} = j^{k+n}$$

$$\beta_{k,n} = e^{j2\pi k\left(-\frac{n}{2}-\frac{L-1}{2M}\right)}$$

$d_{k,n}$ transmitted sequence of the *i*th user (data & pilots) (real)

$x_{k,n}$ observed ideal (without channel) complex sample sequence at AFB output

$$x_{k,n} = \begin{cases} d_{k,n} + ju_{k,n} & \text{for } k+n \text{ even} \\ u_{k,n} + jd_{k,n} & \text{for } k+n \text{ odd} \end{cases}$$

Here $u_{k,n}$ is the un-interesting part of the received complex samples.

$y_{k,n}$ observed channel-distorted complex sample sequence at AFB output

$\tilde{d}_{k,n}$ subcarrier sequence after equalization (real)

$\hat{d}_{k,n}$ detected sequence (real)

$s(m)$ transmitted sequence at SFB output, single user case

$$\begin{aligned} s(m) &= \sum_{k\in\mathsf{M}_u}\sum_{n=-\infty}^{\infty} d_{k,n}\theta_{k,n} g_k\left(m-nM/2\right) \\ &= \sum_{k\in\mathsf{M}_u}\sum_{n=-\infty}^{\infty} d_{k,n}\theta_{k,n} p\left(m-nM/2\right) e^{j\frac{2\pi}{M}k\left(m-n\frac{M}{2}-\frac{L-1}{2}\right)} \\ &= \sum_{k\in\mathsf{M}_u}\sum_{n=-\infty}^{\infty} d_{k,n}\theta_{k,n}(-1)^{kn} p\left(m-nM/2\right) e^{j\frac{2\pi}{M}k\left(m-\frac{L-1}{2}\right)} \\ &= \sum_{k\in\mathsf{M}_u}\sum_{n=-\infty}^{\infty} d_{k,n}\theta_{k,n}\beta_{k,n} p\left(m-nM/2\right) e^{j\frac{2\pi}{M}km} \\ &= \sum_{k\in\mathsf{M}_u}\sum_{n=-\infty}^{\infty} d_{k,n} p_{k,n}(m) \end{aligned}$$

$s_i(m)$ transmitted sequence at SFB output in the uplink multiuser FBMC system, e.g.,

$$s_i(m) = \sum_{k\in\mathsf{M}_u^i}\sum_{n=-\infty}^{\infty} d_{k,n} p_{k,n}(m)$$

$s(t)$ transmitted continuous-time signal ($s_i(t)$ correspondingly for user *i* in multiuser case)

$$s(t) = \sum_{k\in\mathsf{M}_u}\sum_{n=-\infty}^{\infty} d_{k,n}\theta_{k,n}(-1)^{kn} p\left(t-n\frac{T}{2}\right) e^{j2\pi k\left(\Delta f t-\frac{L-1}{2M}\right)}$$

$r(t)$ received continuous-time signal in the uplink multiuser FBMC system

$$r(t) = \sum_{i=1}^{U} e^{j2\pi(\frac{\varepsilon_i}{T}t)} h_i(t,\tau) * s_i(t) + n(t) \qquad \text{general case}$$

$$r(t) = \sum_{i=1}^{U} e^{j2\pi(\frac{\varepsilon_i}{T}t)} \sum_{p=0}^{P_i-1} c_{i,p} s_i(t-\tau_{i,p}) + n(t) \qquad \text{discrete multipath case}$$

$$r(t) = \sum_{i=1}^{U} e^{j2\pi(\frac{\varepsilon_i}{T}t)} c_i s_i(t-\tau_i) + n(t) \qquad \text{AWGN case}$$

$$= \sum_{i=1}^{U} e^{j2\pi(\frac{\varepsilon_i}{T}t+\phi_i)} |c_i| s_i(t-\tau_i) + n(t)$$

ε_i carrier frequency offset of the *i*th user, normalized to subcarrier spacing

ϕ_i carrier phase offset (radians) of the *i*th user in the AWGN model

$h_i(t,\tau)$ time-variant channel impulse response of *i*th user

P_i number of paths in the multipath channel model of user *i*

$c_{i,p}$ complex gain of the *p*th path of the channel of user *i*

$\tau_{i,p}$ delay of the *p*th path of the channel of user *i*

τ_i timing offset of the *i*th user in the AWGN model

$n(t)$ complex envelope of white (Gaussian) noise whose real and imaginary parts are statistically independent and have a power spectral density level of N_0

σ_n^2 channel noise variance

N_0 one-sided noise power spectral density of white channel noise

$r(m)$ received complex sequence at AFB input

$n(m)$ channel noise

$h_i(m)$ discrete-time channel impulse response for user *i* in block-fading model

$H_i(e^{j\omega})$ channel frequency response for user *i*

H_k channel response of subcarrier *k* (assuming flat-fading and time invariant/block-fading case)

$H_{k,n}$ channel response for subcarrier *k* and symbol *n* (assuming flat-fading and time variant case)

$H_{k,n}^{p,q}$ channel response for subcarrier *k* and symbol *n* from TX antenna *p* to RX antenna *q*

$w_k(n)$ subcarrier-wise channel equalizer impulse response for subchannel *k*

Notes:

(1) This assumes causal continuous-time prototype filter impulse response, which is different from Siohan's continuous-time model.

(2) The choice of $\theta_{k,n}$, i.e., the signs in mapping real data sequence to complex samples at the SFB input is an internal choice of the filter bank module (i.e., the definition of $x_{k,n}$ above can be assumed to be valid in any case). However, it has an effect on the signal models at the SFB output and for the complex sequences at the AFB output. In the receiver side, $\beta_{k,n}^*$ is implemented before the subband processing, and $\theta_{k,n}^*$ after it. With this choice, all the subchannels are centered at DC at the subchannel processing stage.

1 Introduction: filter bank based multicarrier (FBMC) transmission principle

Multicarrier transmission techniques based on digital filter banks were developed in the seventies to perform the conversion between PCM (Pulse Code Modulation) and FDM (Frequency Division Multiplexing) systems. In the nineties, OFDM (Orthogonal Frequency Division Multiplexing) was preferred because it was considered simpler in concept, less complex and it had minimum latency. Now, radio communications are moving in directions that make the objections to the filter bank approach unfounded and, in fact, make filter banks particularly attractive. First, in order to achieve quality of service (QoS) and high throughput, radio transmission is resorting to multi-antenna terminals (MIMO), which is a considerable increase in complexity. Moreover, when combined with multicarrier transmission, the MIMO principle requires high resolution spectrum analysis to accurately estimate the channel matrix. Second, communications are migrating to all-IP networks, which implies packet transmission and, therefore, minimum latency at the physical (PHY) layer is no longer crucial and the actual constraints are put on the upper layers. Scalability is a function that is being introduced and it is easily implemented with filter banks because of the independence of sub-channels. In addition, the new concepts of DASM (Dynamic Access Spectrum Management) and cognitive radio require high resolution spectral analysis, a functionality in which filter banks are superior over the discrete Fourier transform of OFDM.

1.1 The filter bank technique

The principle of transmission based on filter banks is shown in Figure 1-1 [1] [2]. The transmitter contains a synthesis filter bank (SFB) and the receiver contains an analysis filter bank (AFB). In the structure of the figure, the FFT (Fast Fourier Transform) is present as in OFDM. It is augmented, to complete a filter bank, by the PPN (Polyphase Network) which consists of a set of digital filters, whose coefficients, globally, form the impulse response of the so-called prototype low-pass filter.

The essential difference between FBMC and OFDM resides in the frequency selectivity. This is illustrated in Figure 1-2, which shows the frequency responses, around a particular sub-carrier, in both cases. OFDM exhibits large ripples in the frequency domain, which imposes the orthogonality constraint between all the sub-carriers. On the contrary, the filter bank frequency response has a negligible amplitude beyond the center frequency of the adjacent sub-carriers. In fact, the filter bank divides the transmission channel of the system into a set of sub-channels and any sub-channel overlaps with its immediate neighbors only. Then, in order to make two groups of contiguous sub-channels independent, it is sufficient to leave a single empty subchannel between them.

The difference in frequency responses between FBMC and OFDM shown in Figure 1-2 has a considerable impact on the performance of wireless systems and their operational flexibility. The FBMC approach has the following features:

- no guard time, or cyclic prefix, is needed,
- full capacity of the transmission bandwidth is achieved using OQAM (Offset Quadrature Amplitude Modulation),
- frequency mask constraints for the transmitted signals are easily satisfied,
- sub-channels can be grouped into independent blocks, which is crucial for scalability and dynamic access, for example,

- with the absence of leakage in the frequency domain, high resolution spectral analysis is achieved,
- the same device can be used in cognitive radio for spectrum sensing and reception, even simultaneously, which guaranties perfect coherence between the two functions.

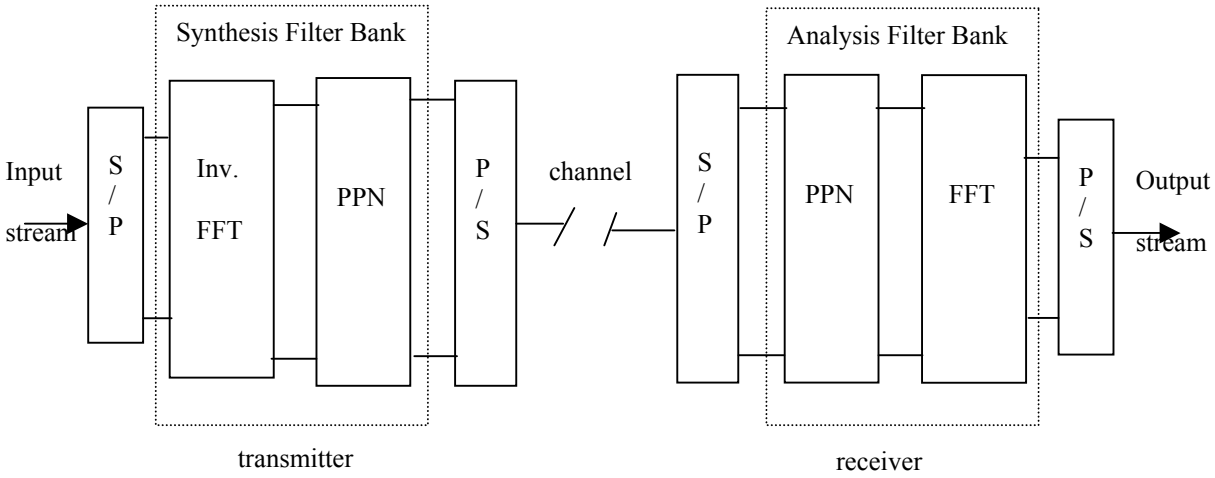

Figure 1-1. Filter Bank-based Multicarrier (FBMC) system

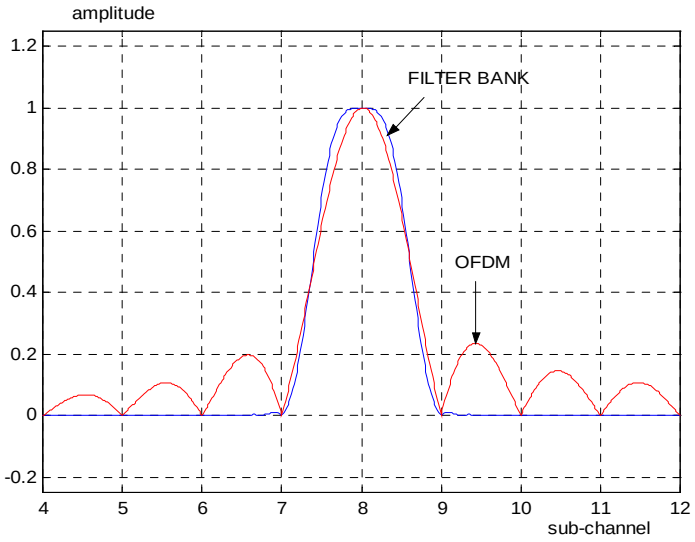

Figure 1-2. Comparison of frequency responses of FBMC and OFDM

2 Description of the reference filter bank

The analysis and synthesis filter banks are naturally the key components in the PHYDYAS project. We start this chapter with a brief discussion concerning general issues related to the choice and characteristics of the filter banks to be used. Then the design method for PHYDYAS reference filter, to be used during the initial phase of the project, is described. In Section 2.3, a more detailed description of the polyphase filter banks structures and related signal models are presented, and in Section 2.4 the characteristics of an ideal FBMC transmission link using the reference filter bank are discussed.

In PHYDYAS, the Work Package 5 is focusing on the further optimization of the filter banks for use during the later phases of the project. The work on filter bank design aspects in the FBMC context will be reported in Deliverable D5.1.

2.1 Choice of filter bank structure

A basic constraint of data transmission is that the channel must satisfy the Nyquist criterion, to avoid intersymbol interference. If the symbol period is T_{symb} and the symbol rate is $f_{symb}=1/T_{symb}$, the channel frequency response must be symmetrical about the frequency $f_{symb}/2$. Accordingly, in FBMC, the prototype filter for the synthesis and analysis filter banks must be half-Nyquist, which means that the square of its frequency response must satisfy the Nyquist criterion.

In this work we consider uniform filter banks, i.e., all the subchannels have the same bandwidth. Efficient uniform filter banks can be implemented using various structures utilizing modulation to create bandpass subchannel filters from a single lowpass prototype filter, basically through frequency-shifting. There are various efficient multirate structures for the needed filter banks, including lapped transforms, lattice structures, and the polyphase structure [3]-[4]. Common to all these structures is that they consist of a filter section, the coefficients of which are determined by the prototype filter design, and a transform section (e.g., discrete Fourier, sine or cosine transforms) implementing the modulation. In combination with the transform blocks, the structures include sampling rate conversion operations, such that the subchannel signals operate at the basic signaling rate, whereas the synthesized wideband signal has a much higer sampling rate.

In a critically sampled filter bank system, the sample rate (counted in terms of real-valued samples in the possible complex (I/Q) signals) of the SFB output and AFB input is equal to the sum of the sample rates of the subchannel signals. In the FBMC application, the use of critically sampled filter banks would be problematic, since the aliasing effects would make it difficult to compensate imperfections of the channel by processing the subchannel signals after the AFB only. Therefore, a factor of two oversampling is commonly applied in the subchannel signals in the AFB. In the considered filter bank models, the useful data symbols are carried alternatingly by real and imaginary parts of the complex-valued subcarrier sequences (in an alternative scheme, the data is in the real parts only [5]). By using the whole complex samples in subchannel processing in the receiver, effectively 2x oversampling is obtained. At the end of the subchannel processing sections, the needed real/imaginary parts are selected to get a critically sampled sequence for detection.

So-called perfect-reconstruction (PR) filter banks implement the Nyquist criterion exactly, and also without introducing any cross-talk between subchannels in the back-to-back connection of SFB and

AFB (so-called transmultiplexer). In wireless communications, the transmission channel introduces inevitably some distortion to the received subchannel signals. Therefore, the PR condition is not essential, and it is sufficient that the cross-talk between subchannels is small enough to be ignored in comparison to the residual interference, e.g., due to imperfect channel equalization. From the filter bank design point of view, this means that the so-called nearly perfect-reconstruction (NPR) designs are sufficient. Since NPR designs are more efficient than PR designs, e.g., in providing higher frequency selectivity with given prototype filter length, NPR designs are the favored choice in PHYDYAS. For NPR filter banks, the polyphase structure is the natural choice, since lapped transforms and lattice structure can be used only in the PR case [3]-[4].

During the first phase of the PHYDYAS project, the work is based on a selected filter bank design known from the literature [2]. This filter bank is based on the polyphase structure and analytical formulas for calculating the filter coefficients for a wide choice of the main parameters:

- The number of subchannels (M) is basically arbitrary, but typically a power of 2 is used in order to be able to use IFFT/FFT as efficient algorithms for the transform blocks.
- Overlapping factor (K) can be selected to be 3 or higher. The basic choice for prototype filter length is $L=KM$, but also $L=KM+1$ or $L=KM-1$ are interesting alternatives.
- The roll-off parameter of this design is essentially $\alpha=1$, which means that the transition bands of a subchannel end at the centers of the adjacent subchannels. This means that only immediately adjacent subchannels are significantly interacting with each other.

2.2 Frequency-sampling based design of prototype filter

A simple technique to design the prototype filter is the so-called frequency sampling technique, which is presented with the following parameters

$$L = 2048 \;;\; M = 512 \;;\; K = 4.$$

The design starts with the determination of L desired values $H(k/L); 0 \le k \le L-1$ in the frequency domain by

$$\begin{aligned} &H(0) = 1 \\ &H(1/L) = 0.971960 \\ &H(2/L) = 1/\sqrt{2} \\ &H(3/L) = \sqrt{1 - H^2(1/L)} = 0.235147 \\ &H(k/L) = 0 \quad ; \quad 4 \le k \le L-1 \end{aligned} \tag{1}$$

Then, the prototype filter coefficients are obtained by inverse DFT as

$$\begin{aligned} &h(m) = 1 + 2\sum_{k=1}^{K-1} (-1)^k H(k/L) \cos(2\pi km/L) \;; \quad 1 \le m \le L-1 \\ &h(0) = 0 \end{aligned} \tag{2}$$

In fact, the condition $h(0) = 0$ determines the desired values $H(1/L)$ and $H(3/L)$. It is useful to make the number of coefficients an odd number, in which case the filter delay can be adjusted to be an integer number of sample periods.

The frequency response obtained is shown in Figure 2-1. In this figure, the sub-channel spacing Δf is taken as unity (Δf=1). It is important to notice that the filter attenuation exceeds 60 dB for the frequency range above 2 sub-channel spacings.

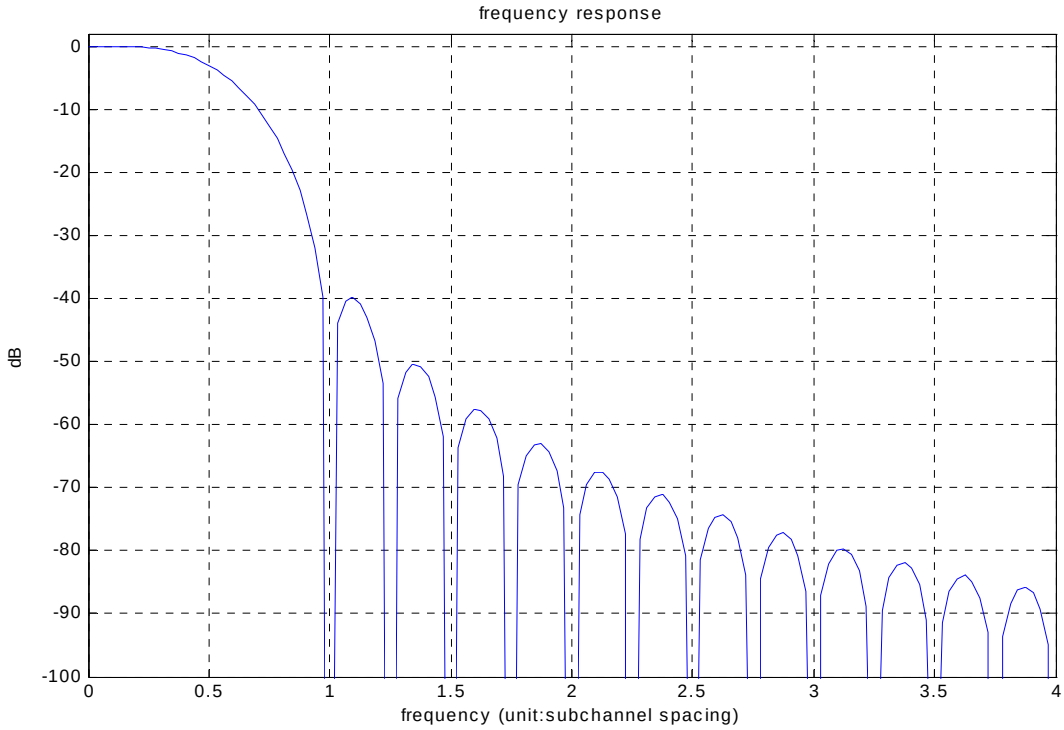

Figure 2-1. Frequency response of the prototype filter

2.3 Polyphase filter bank structure

Figure 2-2 shows the polyphase structures for synthesis and analysis filter banks [1],[3]-[6], including the respective complex-to-real and real-to-complex conversion blocks for transformations between QAM and OQAM symbols. The discrete-time baseband signal at the output of the synthesis bank of an FBMC transmitter based on OQAM modulation can be expressed as

$$s(m) = \sum_{k \in \mathsf{M}_u} \sum_{n=-\infty}^{\infty} d_{k,n} \theta_{k,n} g_k \left(m - nM/2 \right) \tag{3}$$

where $d_{k,n}$ is the transmitted sequence of the ith user, and

$$\theta_{k,n} = j^{(k+n)}. \tag{4}$$

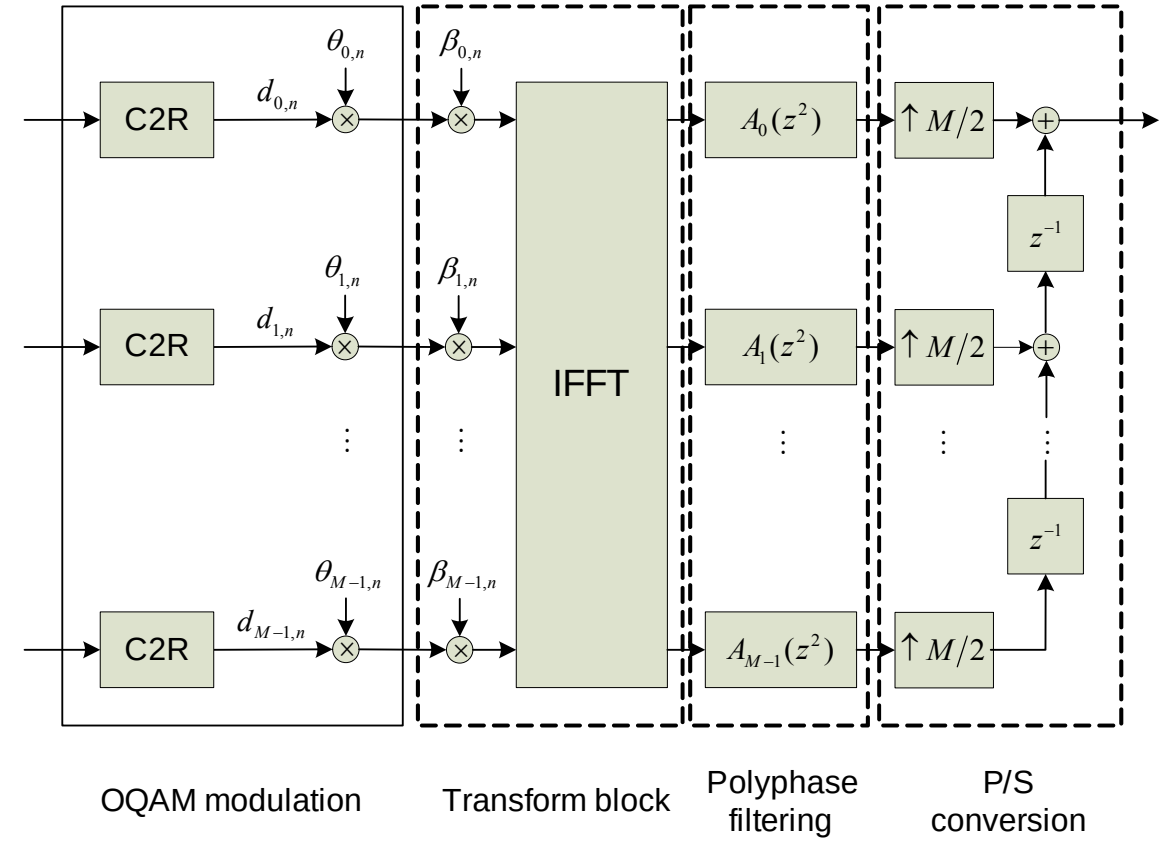

(a)

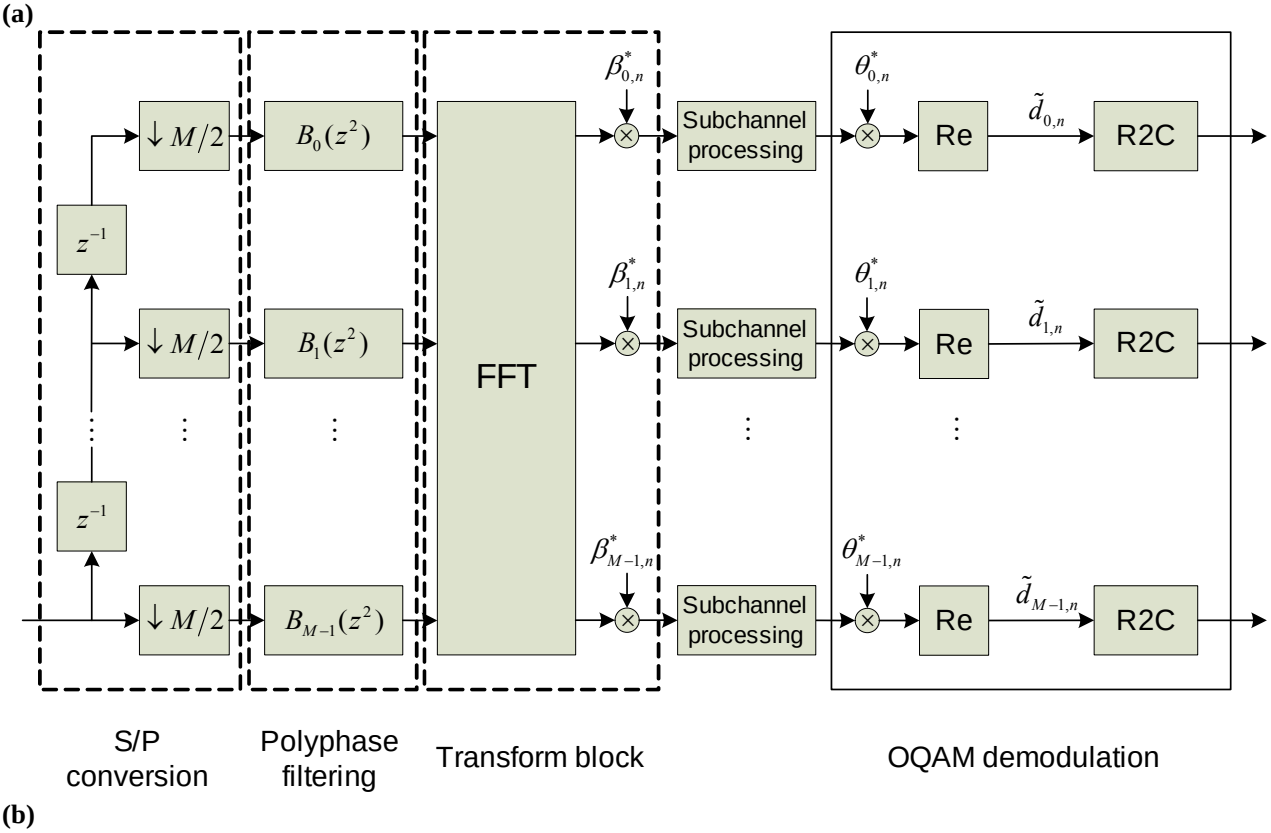

(b)

Figure 2-2. Polyphase filter bank structures. (a) Synthesis bank (SFB). (b) Analysis bank (AFB).

Here M is the overall number of subcarriers (=IFFT/FFT size), M_u is the set of active subcarriers, and $d_{k,n}$ denotes the real-valued symbols at the kth subcarrier during the nth symbol interval, modulated at rate $2/T$. The signaling interval T is defined as the inverse of the subcarrier spacing, i.e., $T = 1/\Delta f$. The symbols $d_{k,n}$ and $d_{k,n+1}$ can be interpreted to carry the In-phase and Quadrature (I/Q) components of the complex-valued symbol $c_{k,l}$ (of rate $1/T$) from a QAM-alphabet. It should be noted that the signs of the $\theta_{k,n}$ sequence can be chosen arbitrarily, but the pattern of real and imaginary samples has to follow this definition to maintain (near) orthogonality [1].

In (3), $g_k(m)$ are shift-invariant impulse responses of the SFB channel filters. The signal model can also be written in terms of the prototype filter impulse response, $p(m)$ of length L, as follows:

$$\begin{aligned} s(m) &= \sum_{k\in\mathsf{M}_u}\sum_{n=-\infty}^{\infty} d_{k,n}\theta_{k,n}\, p\left(m - nM/2\right) e^{j\frac{2\pi}{M}k\left(m - n\frac{M}{2} - \frac{L-1}{2}\right)} \\ &= \sum_{k\in\mathsf{M}_u}\sum_{n=-\infty}^{\infty} d_{k,n}\theta_{k,n}\beta_{k,n}\, p\left(m - nM/2\right) e^{j\frac{2\pi}{M}km} \end{aligned} \tag{5}$$

where

$$\beta_{k,n} = e^{-jkn\pi}\cdot e^{-j\frac{k}{M}(L-1)\pi} = (-1)^{kn}\cdot e^{-j\frac{k}{M}(L-1)\pi} \tag{6}$$

From the latter form of (5), the different parts of the polyphase SFB structure of Figure 2-2(a) can be identified.

We can use also the following short-hand notation for the signal model:

$$s(m) = \sum_{k\in\mathsf{M}_u}\sum_{n=-\infty}^{\infty} d_{k,n}\, p_{k,n}(m) \tag{7}$$

where

$$p_{k,n}(m) = \theta_{k,n}\beta_{k,n}\, p\left(m - nM/2\right) e^{j\frac{2\pi}{M}km}. \tag{8}$$

The synthesized signal burst is therefore a composite of multiple subchannel signals each of which consists of a linear combination of time-shifted (by multiples of $T/2$) and overlapping impulse responses of the prototype filter, weighted by the respective symbol values $d_{k,n}$.

The continuous-time model for the transmitted waveform can be written as

$$s(t) = \sum_{k\in\mathsf{M}_u}\sum_{n=-\infty}^{\infty} d_{k,n}\theta_{k,n}(-1)^{kn}\, p\left(t - n\frac{T}{2}\right) e^{j2\pi k\left(\Delta f t - \frac{L-1}{2M}\right)} \tag{9}$$

where $p(t)$ is the continuous-time impulse response corresponding to the prototype filter design.

2.4 Model for ideal FBMC transmission link

The transmultiplexer, i.e., the back-to-back connection of an SFB and AFB, is a fairly complicated multirate signal processing structure, and the expression of the AFB output subchannel samples in terms of the SFB subchannel samples and prototype filter impulse response is rather complicated. It is not included here, but we present a simplified model instead. In case of ideal channel, the complex oversampled subchannel signals in AFB can be expressed as

$$x_{k_0,n_0} = \sum_{k \in \mathsf{M}_u} \sum_{n=-\infty}^{\infty} d_{k,n} \theta_{k,n} t_{k_0-k.n_0-n} \tag{10}$$

The transmultiplexer response, $t_{k,n}$, is determined by the filter bank design. The transmultiplexer response of the reference filter bank system is illustrated in Table 2-1.

Table 2-1. Transmultiplexer response of the FBMC system using PHYDYAS reference bank

time / sub-ch.	-4	-3	-2	-1	*0*	1	2	3	4
-2	0	0.0006	-0.0001	0	0	0	-0.0001	0.0006	0
-1	0.0054	j.0429	-0.1250	-j.2058	0.2393	j.2058	-0.1250	-j.0429	0.0054
0	0	-0.0668	0.0002	0.5644	**1**	0.5644	0.0002	-0.0668	0
1	0.0054	-j.0429	-0.1250	j.2058	0.2393	-j.2058	-0.1250	j.0429	0.0054
2	0	0.0006	-0.0001	0	0	0	-0.0001	0.0006	0

It can be seen that the effect of subchannel *k* in the second adjacent subchannels (*k*-2, *k*+2) is very small. In the time direction, the effect of sample at time *n* extends to the range *n*-4 … *n*+4, due to the overlapping factor of 4.

The non-orthogonality (due to NPR design) can be seen in the samples (*k*±2, *n*±2), (*k*, *n*±2), which are quite small in magnitude. The resulting background noise of the system is at the level of $\sigma_b^2 = -65\,\mathrm{dB}$ assuming that the subchannel signal variance is 1.

3 Synchronization and initialization in FBMC transmission

The trend in communications is toward all-IP networks and future radio communications and wireless networks are likely to be based on packet transmission. Basically, a packet contains two sections, namely a preamble which is used for the initialization and synchronization of the receiver and the data payload, during which the receiver is finely tuned and the evolutions of the channel are tracked to maximize the global throughput. In FBMC, two different contexts must be distinguished: full block processing and group of subchannels. The synchronization issues in both modes of operation are presented in this section in a global view.

Another important issue in the initialization (and termination) of an FBMC transmission burst is due to the fact that the basic signaling waveforms, corresponding to symbols transmitted at different time instances, are overlapping and longer than in the OFDM case. In general, with overlapping factor K, the length of the waveform corresponding to one OQAM symbol is K+1/2 times the OQAM symbol interval. This would introduce a significant overhead if the 'burst tails' were to be fully accommodated in the transmission frame. This issue will be discussed later in Chapter 6.

3.1 Full block processing

This is the case of downlink transmission and time-division multiple access (TDMA) based uplink, for example, and the situation is similar to OFDM. All the sub-channels are synchronous and most of the processing can be carried out in the time domain. The functions involved are shown in Figure 3-1.

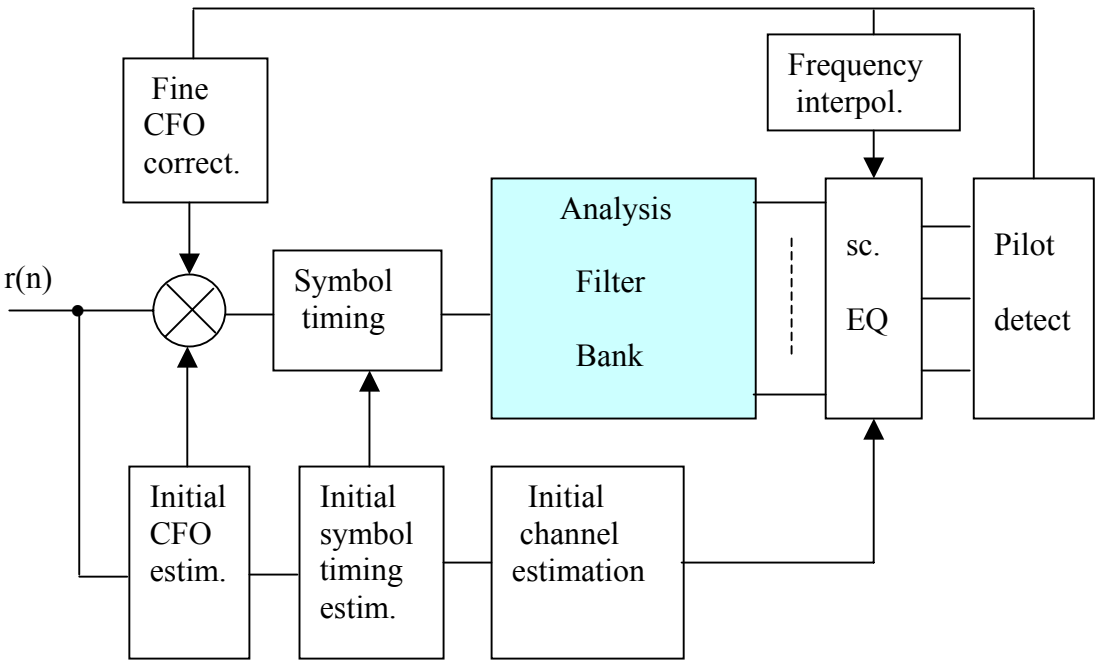

Figure 3-1. Block diagram of the full block FBMC receiver

The training sequence is designed to provide estimates for the initial carrier frequency offset (CFO), the symbol timing, and the channel frequency response. These estimations can be derived sequentially or simultaneously. The CFO correction is applied to the received sequence $r(n)$. The initial symbol timing alignment greatly simplifies the equalization task because it eliminates the need for interpolation in the sub-channel equalizers. The channel estimation is exploited to determine the structure of the sub-channel equalizers and the coefficient values. The channel estimation methods are discussed in PHYDYAS Deliverable D3.1 [7]. It must be pointed out that the latency of the equalizers must be minimized so that the total latency of the system remains tolerable.

During payload transmission, the residual CFO must be corrected and the evolutions of the channel must be tracked. Pilot signals can be inserted to that purpose, as in OFDM. The updating of the equalizer coefficients can be derived through frequency domain interpolation. The presence of pilots reduces the global throughput and their number must be kept as small as possible. An alternative approach consists in exploiting the detected symbols in a decision directed mode.

3.2 Group of sub-channels

This configuration occurs in frequency-division multiple access (FDMA) based uplink transmission, for example, when a symbol is exploited by several non-synchronous users and the processing must be done in the frequency domain, as illustrated in
Figure 3-2

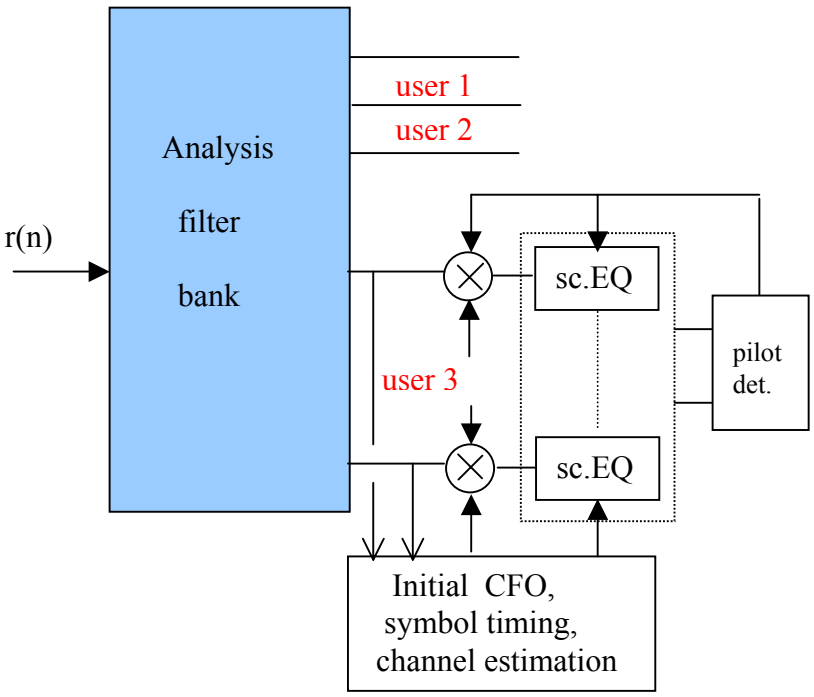

Figure 3-2. Block diagram of the receiver section for a group-of-subchannels

The initialization information for user 3 has to be obtained from the signals coming out of the sub-channels allocated to this user. For estimation purposes, the signals of all the sub-channels can be exploited jointly, but the corrections are implemented per sub-channel. The CFO correction and

delay compensation functions are common for all subchannels of a user, but the channel equalizers are different for different sub-channels. The delay compensation can be implemented using fractional delay filters/interpolators, or using the subcarrier equalizers, if multitap subcarrier equalizers of sufficient length are employed. The CFO and delay compensation methods, as well as channel estimation and equalization methods are discussed in detail in [7], whereas this report focuses on the estimation of the synchronization parameters.

Frequency-domain methods for CFO and delay estimation are primarily motivated by the FDMA based uplink where this is the only sensible alternative. This is because for time-domain methods, the different uplink user bands should be separated by filters which would need to be highly frequency selective. For frequency-domain methods, the analysis filter bank separates the users in a natural way, without need for any additional processing blocks.

Regarding the full-block transmission mode, similar issues make the frequency-domain estimation methods an interesting alternative, especially in the cognitive radio scenarios. If the used signal band is discontinuous or if it contains significant narrowband interferences, the situation regarding the channelization filtering for possible time-domain functionalities is similar to that in the FDMA uplink scenario. Furthermore, in an FBMC receiver, the final stage of the actual channelization filtering can be done by the analysis filter bank, and the baseband filtering can be relaxed. Also the received signal band can be easily and rapidly configured just by selecting the subchannels that are in use during a particular transmission slot. In such scenarios, the AFB can also be used for suppressing interferences or other user signals, whereas the frequency selectivity needed for time-domain functionalities would require significant additional processing at baseband.

One approach for preamble-based synchronization and channel estimation in FBMC transmission was presented in [8]. However, this approach requires fairly long preambles (3-5 OQAM symbols), and one of the main targets in the current work is to reduce the training overhead in FBMC systems.

Even though the importance of frequency-domain methods for estimating the synchronization parameters is emphasized here, it is important to develop also time-domain techniques. They would be feasible in many basic scenarios and might have lower implementation complexity because the filter bank processing could be avoided during the initialization phase.

4 Data-Aided Synchronization and Initialization

4.1 Preamble-based time & frequency initialization for full-block scheme.

To allow for an efficient implementation of the receiver, and lower the equalizer complexity, accurate time/frequency offset knowledge should be acquired in the time domain, i.e., before running the receiver filter bank.

An initialization scheme for data-aided symbol timing and carrier frequency offset recovery with robust acquisition properties in dispersive channels has been derived. Specifically, this algorithm exploits the known structure of a training sequence made up of identical parts. The proposed method is based on the least squares (LS) approach, it operates in the time domain before running the receiver filter bank, and, moreover, it does not require the knowledge of the channel impulse response and of the signal-to-noise ratio (SNR).

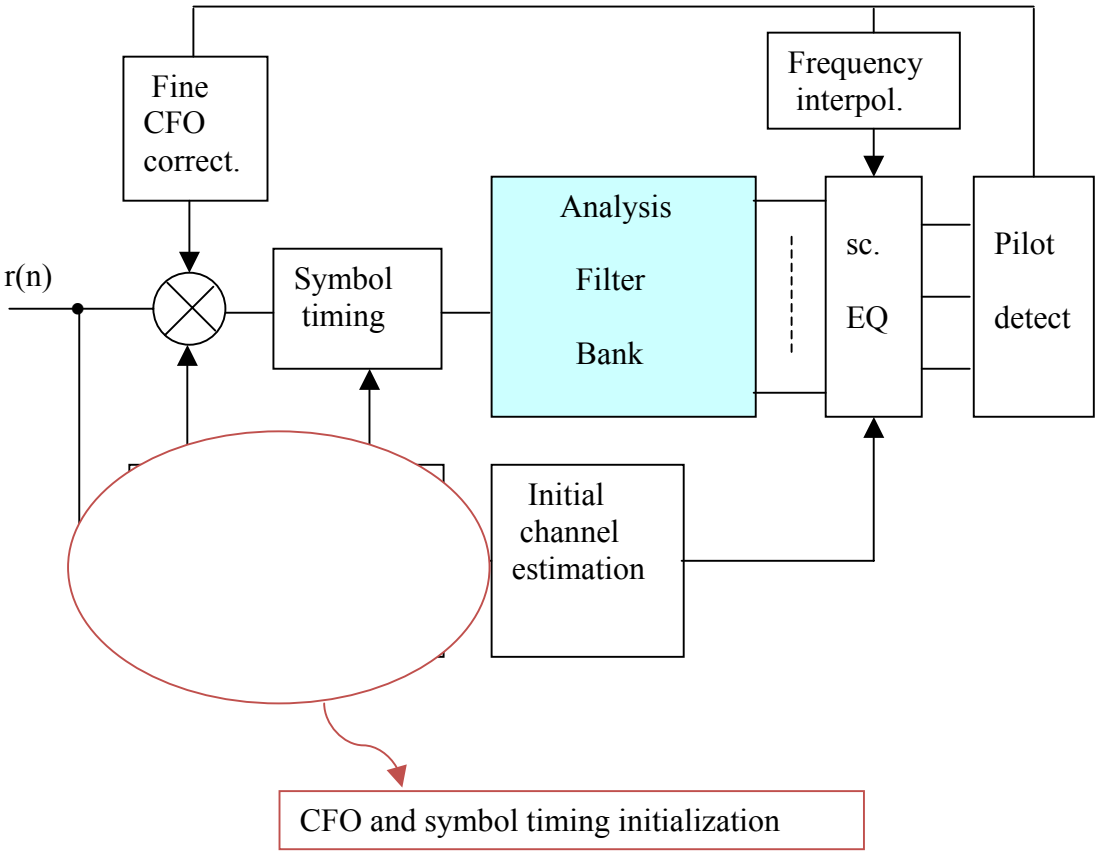

Figure 4-1. Block diagram of the full block FBMC receiver

4.1.1 Proposed estimator

The proposed data-aided joint CFO and symbol timing estimator [10] is based on the LS approach and exploits the transmission of a training sequence made up of identical blocks. Precisely, the training sequence can be obtained by transmitting the sequence of data symbols $d_{k,n} = d_k^{TR}$ $\forall k \in \mathcal{M}_u$ and $\forall n \in \{0,...,2N_{TR}-1\}$. In this way, if the pulse shaping filter $p(t)$ is different from zero for $t \in \{0, T_s, ..., (L-1)T_s\}$, where $L = K\,T/T_s$ the training sequence is given by

$$s_{TR}(mT_s) = \sqrt{\frac{M}{2M_u}} \sum_{k \in M_u} \sum_{n=0}^{2N_{TR}-1} d_k^{TR} \theta_{k,n} \beta_{k,n} p\left(mT_s - nT/2\right) e^{j\frac{2\pi}{M}km}. \tag{11}$$

After a transient of $L-1$ samples[1] and, in particular for $m \in \{L-1, ..., N_{TR}M - M - 1\}$, the training sequence satisfies the following relationship

$$s_{TR}(mT_s) = s_{TR}(mT_s + MT_s). \tag{12}$$

The transmitted sequence $s(mT_s)$ feeds a digital-to-analog converter (DAC) and propagates trough a physical channel characterized by AWGN noise $n(t)$. The received signal $r(t)$ is filtered with an ideal low-pass filter with a bandwidth of $1/T_s$ and sampled with a frequency $f_s = 1/T_s$, yielding the sequence

$$r(mT_s) = e^{j2\pi\left(\frac{\varepsilon_0}{T} mT_s\right)} c_0 s(mT_s - \tau_0) + n(mT_s) \tag{13}$$

Accounting for (12) a joint symbol timing and CFO estimator can be obtained by considering the minimization problem

$$(\hat{\varepsilon}_0, \hat{\tau}_0) = \arg\min_{(\tilde{\varepsilon}_0, \tilde{\tau}_0)} \left\{ \sum_{m=L-1}^{M(N_{TR}-1)-1} \left| r(mT_s + \tilde{\tau}_0) - r(mT_s + MT_s + \tilde{\tau}_0) e^{-j2\pi\tilde{\varepsilon}_0} \right|^2 \right\} \tag{14}$$

where $\tilde{\varepsilon}_0$ and $\tilde{\tau}_0$ are trial values for CFO and symbol timing, respectively. The minimization in (14) leads to the following joint CFO and symbol timing estimator referred to as LS estimator

$$\hat{\tau}_{LS} = \arg\max_{\tilde{\tau}_0} \left\{ 2\left|R(\tilde{\tau}_0)\right| - Q(\tilde{\tau}_0) \right\} \tag{15}$$

and

$$\hat{\varepsilon}_{LS}(\hat{\tau}_{LS}) = \frac{1}{2\pi} \angle\left\{ R(\hat{\tau}_{LS}) \right\} \tag{16}$$

with

$$R(\tilde{\tau}_0) \overset{\Delta}{=} \sum_{m=L-1}^{M(N_{TR}-1)-1} r^*(mT_s + \tilde{\tau}_0) r(mT_s + MT_s + \tilde{\tau}_0) \tag{17}$$

and

$$Q(\tilde{\tau}_0) \overset{\Delta}{=} \sum_{m=L-1}^{M(N_{TR}-1)-1} |r(mT_s + \tilde{\tau}_0)|^2 + \sum_{m=L-1}^{M(N_{TR}-1)-1} |r(mT_s + MT_s + \tilde{\tau}_0)|^2 . \tag{18}$$

Let us observe that if we divide the timing metric in (15) by $Q(\tilde{\tau})$ we obtain the joint symbol timing and CFO estimator

[1] The transient can be avoided if preloading techniques are used.

$$\hat{\tau}_{MTR1} = \arg\max_{\tilde{\tau}_0} \left\{ \frac{2\left|R(\tilde{\tau}_0)\right|}{Q(\tilde{\tau}_0)} \right\} \tag{19}$$

and

$$\hat{\varepsilon}_{MTR1}(\hat{\tau}_{MTR1}) = \frac{1}{2\pi} \angle \left\{ R(\hat{\tau}_{MTR1}) \right\}. \tag{20}$$

The joint estimator in (19) and in (20) represents a modified version of the synchronization algorithm for FMT systems proposed by Tonello and Rossi in [10] and it is referred to as modified Tonello Rossi 1 (MTR1). In [10] it is also considered a joint symbol timing and CFO estimator for AWGN channel exploiting the knowledge of a pseudo-noise sequence. This synchronization algorithm referred to as MTR2 can be obtained by considering the minimization problem

$$\begin{aligned}(\hat{\varepsilon}_{MTR2}, \hat{\tau}_{MTR2}) = \quad & \arg\min_{\tilde{\varepsilon}_0, \tilde{\tau}_0} \left\{ \sum_{m=L-1}^{N_{TR}M-M-1} \left| s_{TR}^*(mT_s) s_{TR}(mT_s + MT_s) \right.\right. \\ & \left.\left. - r^*(mT_s + \tilde{\tau}_0) r(mT_s + MT_s + \tilde{\tau}_0) e^{-j2\pi\tilde{\varepsilon}_0} \right|^2 \right\}.\end{aligned} \tag{21}$$

After simple algebraic manipulations we obtain the joint symbol timing and CFO estimator

$$\hat{\tau}_{MTR2} = \arg\max_{\tilde{\tau}_0} \left\{ \frac{2\left|S(\tilde{\tau}_0)\right|}{T(\tilde{\tau}_0)} \right\} \tag{22}$$

$$\hat{\varepsilon}_{MTR2}(\hat{\tau}_{MTR2}) = \frac{1}{2\pi} \angle \left\{ S(\hat{\tau}_{MTR2}) \right\} \tag{23}$$

with

$$S(\tilde{\tau}_0) = \sum_{m=L-1}^{N_{TR}M-M-1} r^*(mT_s + \tilde{\tau}_0) s_{TR}(mT_s) r(mT_s + MT_s + \tilde{\tau}_0) s_{TR}^*(mT_s + MT_s) \tag{24}$$

and

$$T(\tilde{\tau}_0) = \sum_{m=L-1}^{N_{TR}M-M-1} |s_{TR}(mT_s)|^2 |s_{TR}(mT_s + MT_s)|^2 + \sum_{m=L-1}^{N_{TR}M-M-1} |r(mT_s + \tilde{\tau}_0)|^2 |r(mT_s + \tilde{\tau}_0 + MT_s)|^2 . \tag{25}$$

It is worthwhile to note that the considered LS, MTR1 and MTR2 CFO estimators in (16), (20) and (23), respectively, provide a closed form solution for the CFO estimate and do not require the knowledge of the channel impulse response and of the SNR. Moreover, they can assure unambiguous CFO estimates if $|\varepsilon_0| < 1/2$. On the other hand, the considered LS, MTR1 and MTR2 symbol timing estimators do not present a closed form solution but they require a maximization with respect to the continuous parameter $\tilde{\tau}_0$.

4.1.2 Numerical results OFDM/OQAM systems

The performance of the joint LS symbol timing and CFO estimator is compared with that of the data-aided synchronization algorithms MTR1 and MTR2.
A number of 10^4 Monte Carlo trials has been performed under the following conditions:

- The value of the normalized CFO, of the timing offset and of the carrier phase are fixed at $\varepsilon_0=0.03$, $\tau_0=3T_s$ and $\varphi_0=\pi/8$, respectively.
- The size of the set of subcarriers is M=1024 while the number of virtual subcarriers is $M_v=128$.
- The prototype filter is that described in Section 2 with an overlapping factor K=4.
- Numerical results have been obtained by considering two different scenarios: AWGN channel and multipath channel modeled using the Vehicular-A channel model of ITU-R.

Figure 4-2 and Figure 4-3 show the root mean squared error (RMSE) of the considered joint CFO and symbol timing estimators in AWGN (solid lines) and multipath channel (dashed lines) as a function of the SNR in dB, for a training sequence with $N_{rip}=2$ identical blocks each of length *M*. In the figures is also included the Cramér-Rao bound (CRB) for CFO and symbol timing estimation, whose derivation details are reported in [11]. The results show that in AWGN channel the MTR2 symbol timing estimator exhibits the best performance for all the considered SNR values, while the considered CFO estimators exhibit nearly the same performance providing an RMSE close to the CRB.

In multipath channel, the LS and MTR1 CFO and symbol timing estimators assure the lowest RMSE and exhibit a contained performance loss with respect to that achieved in AWGN, while the MTR2 symbol timing estimator presents a severe performance degradation. As shown in Figure 4-3 the considered CFO estimators assure a particular robustness in the presence of multipath channel, providing a performance very close with that achieved in AWGN channel.

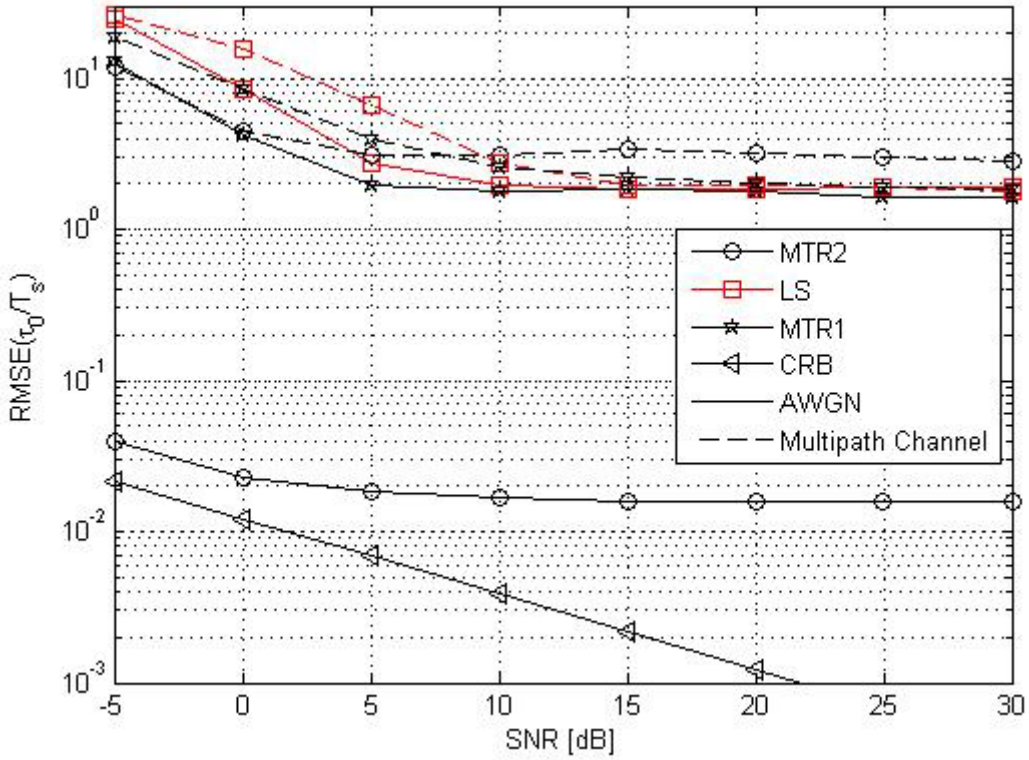

Figure 4-2. Performance of the considered symbol timing estimators in AWGN and multipath channel.

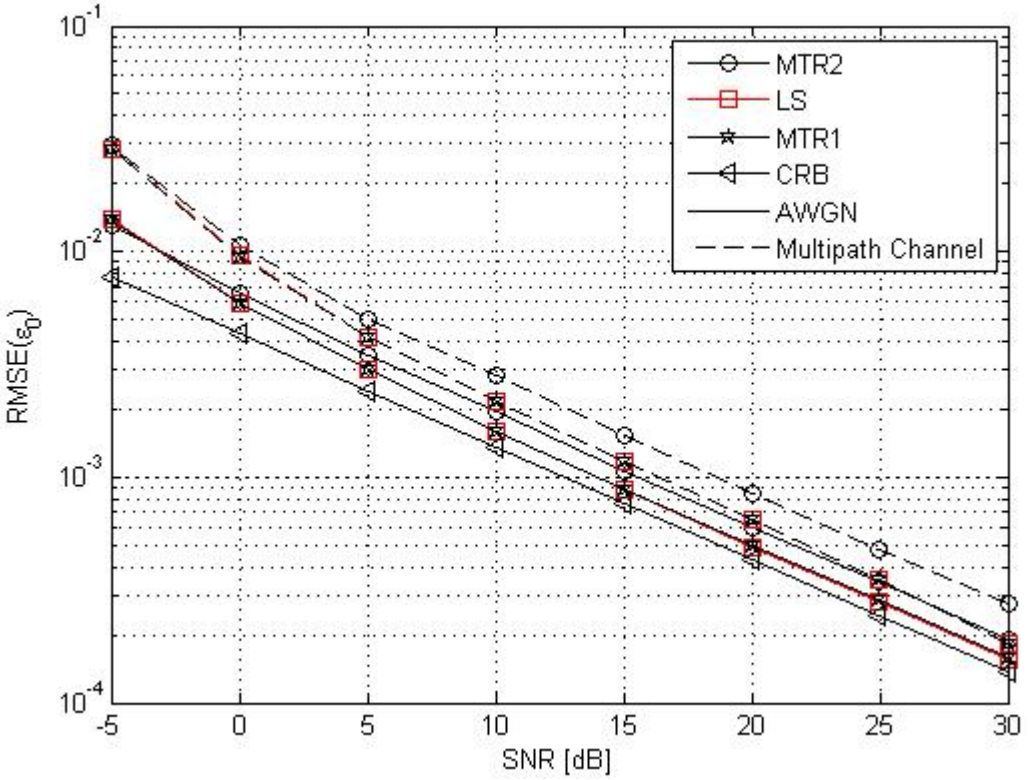

Figure 4-3. Performance of the considered CFO estimators in AWGN and multipath channel.

4.1.3 Comparison with OFDM system

In this section we evaluate the performance of a joint symbol timing and CFO estimation algorithm exploited for OFDM systems.

Precisely, in this case the training sequence is made up of two identical parts, obtained by transmitting pseudonoise data symbols on the subcarriers with even indices and setting zero on the remaining subcarriers. In this way, we obtain the training sequence

$$s_{TR}(mT_s) = \sum_{l \in A} a_l^{TR} e^{jl\frac{2\pi}{M}m} \tag{26}$$

made up of two identical parts, that is,

$$s_{TR}(mT_s) = s_{TR}(mT_s + MT_s/2). \tag{27}$$

Accounting for the redundancy of the training sequence a joint symbol timing and CFO estimator can be obtained by considering the minimization problem

$$(\hat{\varepsilon}_0, \hat{\tau}_0) = \arg\min_{(\tilde{\varepsilon}_0, \tilde{\tau}_0)} \left\{ \sum_{m=0}^{M/2-1} \left| r(mT_s + \tilde{\tau}_0) - r(mT_s + MT_s/2 + \tilde{\tau}_0) e^{-j\pi\tilde{\varepsilon}_0} \right|^2 \right\}. \tag{28}$$

The minimization in (28) leads to the following joint CFO and symbol timing estimator

$$\hat{\tau} = \arg\max_{\tilde{\tau}_0} \left\{ 2\left|U(\tilde{\tau}_0)\right| - V(\tilde{\tau}_0) \right\} \tag{29}$$

and

$$\hat{\varepsilon}(\hat{\tau}) = \frac{1}{\pi} \angle \left\{ U(\hat{\tau}) \right\} \tag{30}$$

with

$$U(\tilde{\tau}_0) \overset{\Delta}{=} \sum_{m=0}^{M/2-1} r^*(mT_s + \tilde{\tau}_0) r(mT_s + MT_s/2 + \tilde{\tau}_0) \tag{31}$$

and

$$V(\tilde{\tau}_0) \overset{\Delta}{=} \sum_{m=0}^{M/2-1} |r(mT_s + \tilde{\tau}_0)|^2 + \sum_{k=0}^{M/2-1} |r(mT_s + MT_s/2 + \tilde{\tau}_0)|^2 . \tag{32}$$

Let us observe that if we divide the timing metric in (29) by $V(\tilde{\tau}_0)$ we obtain a joint symbol timing and CFO estimator similar to that derived in [12] by Schmidl and Cox and referred in the following to as modified Schmidl and Cox estimator

$$\hat{\tau}_{MSC} = \arg\max_{\tilde{\tau}_0} \left\{ \frac{2\left|U(\tilde{\tau}_0)\right|}{V(\tilde{\tau}_0)} \right\} \tag{33}$$

and

$$\hat{\varepsilon}_{MSC}(\hat{\tau}_{SC}) = \frac{1}{\pi} \angle \left\{ R(\hat{\tau}_{MSC}) \right\}. \tag{34}$$

In the following the performance of the considered estimator is assessed via numerical simulations by considering a number of 10^4 Monte Carlo trials performed under the following conditions:

- The value of the normalized CFO, the timing offset and the carrier phase are fixed at $\varepsilon_0=0.03$, $\tau_0=3T_s$ and $\varphi_0=\pi/8$, respectively.
- The size of the set of subcarriers for the considered OFDM is M=2048 while the cyclic prefix length is CP=256.
- The training symbol is obtained by considering an OFDM symbol with two identical parts each of length M/2=1024 (that is the length of each part is equal to that of the OFDM/OQAM training symbol used in the subsection 4.1.1).
- The multipath channel has been modeled using the Vehicular-A channel model of ITU-R.

In Figure 4-4 and Figure 4-5 is shown the performance of the considered joint MSC symbol timing and CFO estimator, respectively, in AWGN (solid lines) and multipath channel (dashed lines) as a function of the SNR. The results show that the MSC estimator assures in all the considered scenarios symbol timing and CFO estimates less accurate than that provided by the LS and MTR1 estimators for OFDM/OQAM systems (see Figure 4-2 and Figure 4-3).

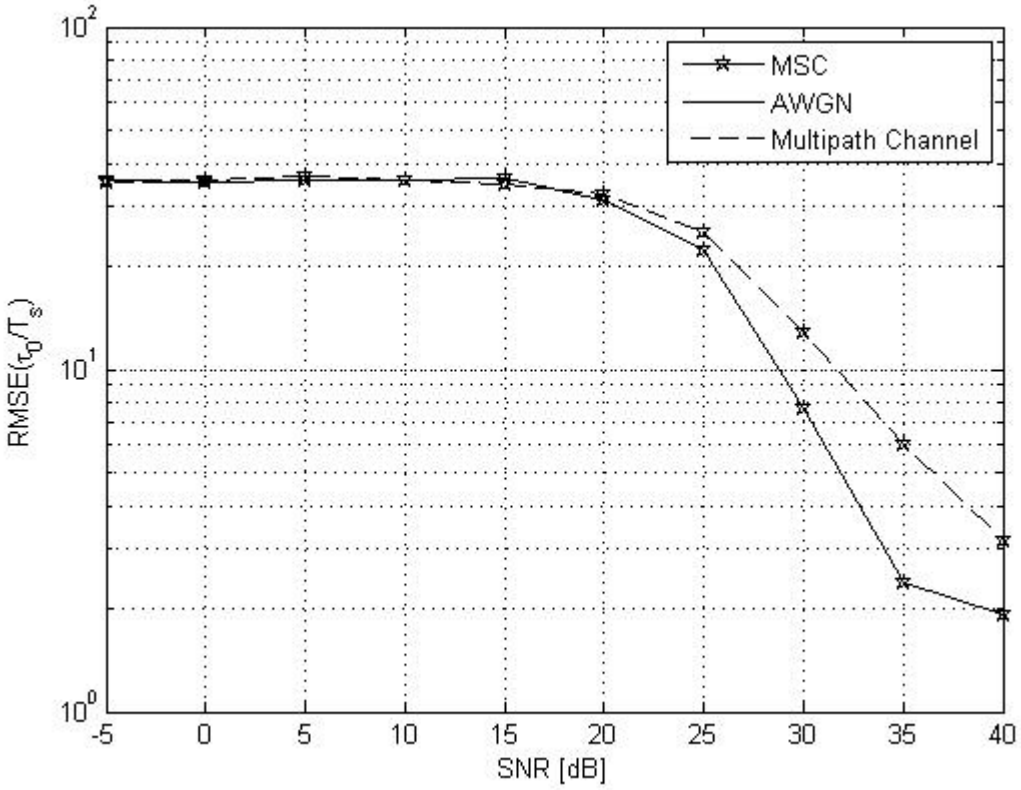

Figure 4-4. Performance of the considered MSC symbol timing estimator in AWGN and multipath channel.

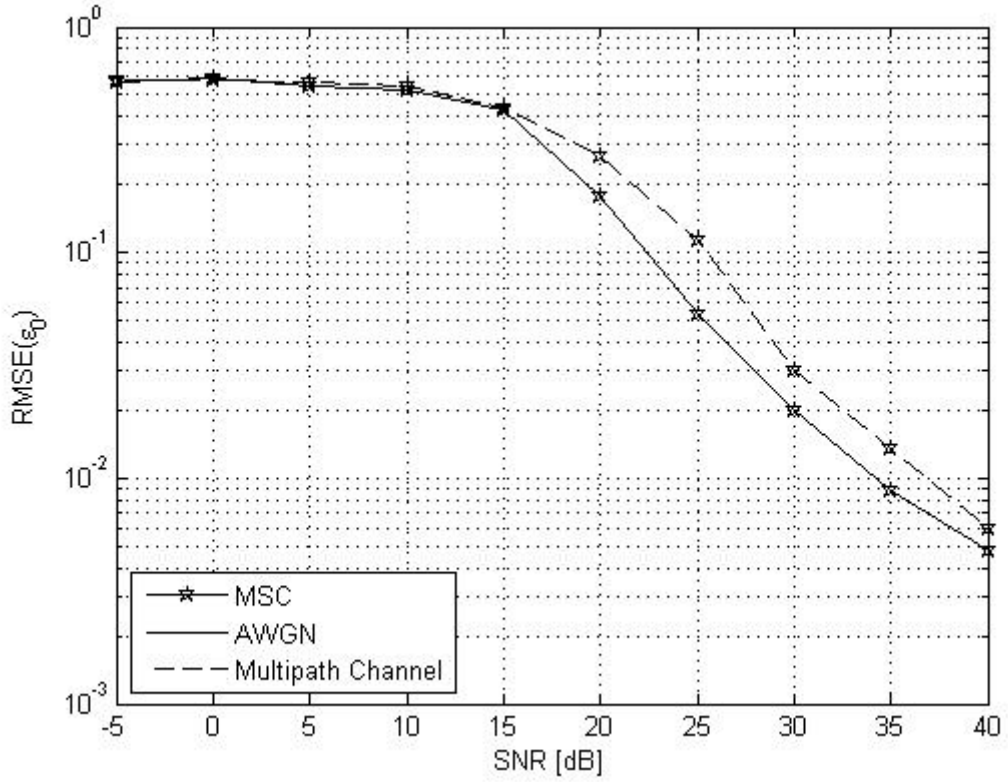

Figure 4-5. Performance of the considered MSC CFO estimator in AWGN and multipath channel.

4.2 Preamble-based synchronization and initialization for uplink

Preamble-based synchronization techniques can also be used in the uplink of a multiuser OFDM/OQAM system. Specifically, in section 4.2.1 (section 4.2.2) the joint maximum likelihood (ML) phase offset and symbol timing estimator (joint ML phase offset and CFO estimator), exploiting a short known preamble embedded in the burst received from each of *U* users, is derived. Since the waveforms of the different users are nearly orthogonal, the ML approach leads to *U* different joint phase offset and symbol timing (CFO) estimators. Moreover, for each user the phase estimate is in closed form, and, then, the symbol timing (CFO) estimator requires only a one-dimensional maximization procedure with respect to a continuous parameter. The performance of the proposed ML estimators is assessed via computer simulations both in AWGN and multipath channel.

4.2.1 ML symbol timing estimator

In this section we derive the joint ML phase and timing estimator for uplink OFDM/OQAM systems with perfect carrier-frequency synchronization, by exploiting the transmission of a training sequence, embedded in the transmitted burst. In particular, let us consider a preamble of N_{TR} OFDM/OQAM symbols, the training sequence of the *i*th user, is given by

$$z_i(mT_s) = \sum_{k\in M_u^i} \sum_{n=0}^{2N_{TR}-1} d_{k,n}\theta_{k,n}\beta_{k,n}p\left(mT_s - nT/2\right)e^{j\frac{2\pi}{M}km} \tag{35}$$

The received signal in AWGN channel, when the information-bearing of the *i*th $s_i(mT_s)$ presents a timing offset τ_i, a carrier phase offset ϕ_i and an attenuation $|c_i|$, can be expressed as

$$r(mT_s) = \sum_{i=1}^{U} e^{j2\pi\phi_i}\left|c_i\right| z_i(mT_s - \tau_i) + n(mT_s) \tag{36}$$

By considering an observations window of total length $N\eta$ containing the non-zero support of the preamble received from each user, the likelihood function in AWGN channel for the unknown parameters $\{\tau_i\}_{i=1}^{U}$ and $\{\phi_i\}_{i=1}^{U}$ is given by (up to an irrelevant multiplicative factor)

$$\Lambda\left(\underline{\tau},\underline{\varphi}\right) = \exp\left\{-\frac{T_s}{N_0}\sum_{m=0}^{\eta M-1}\left|r(mT_s) - \sum_{i=1}^{U}|c_i|\,e^{j2\pi\tilde{\varphi}_i}\tilde{z}_i^{\tilde{\tau}_i}(mT_s)\right|^2\right\} \tag{37}$$

where $\underline{\tau} = \left(\tau_1,\tau_2,...,\tau_U\right)$, $\underline{\varphi} = \left(\varphi_1,\varphi_2,...,\varphi_U\right)$,

$$\begin{aligned} z_i^{\tau_i}(mT_s) &= z_i(mT_s - \tau_i) \\ &= \sum_{k\in M_u^i}\sum_{n=0}^{2N_{TR}-1} d_{k,n}\theta_{k,n}\beta_{k,n}p\left(mT_s - nT/2 - \tau_i\right)e^{j\frac{2\pi}{T}k(mT_s-\tau_i)} \end{aligned} \tag{38}$$

and the notation of the type $\tilde{x}$ indicates trial value of x.

By replacing (38) in (37) and dropping irrelevant multiplicative and additive factors we get

$$\ln \Lambda\left(\underline{\tau},\underline{\varphi}\right)=\sum_{i=1}^{U}\mathrm{Re}\left[Z_i\left(\tilde{\varphi}_i,\tilde{\tau}_i\right)\right] \tag{39}$$

where

$$Z_i\left(\tilde{\varphi}_i,\tilde{\tau}_i\right)=|c_i|e^{-j2\pi\tilde{\varphi}_i}\sum_{m=0}^{\eta M-1}r(mT_s)\tilde{z}_i^{\tilde{\tau}_i}(mT_s)^*. \tag{40}$$

In particular, in the derivation of (39), we have neglected the quantity

$$\sum_{m=0}^{\eta M-1}\left|\sum_{i=1}^{U}\left|c_i\right|e^{j2\pi\tilde{\phi}_i}\tilde{z}_i^{\tilde{\tau}_i}\left(mT_s\right)\right|^2=C_1+C_2 \tag{41}$$

since it is weakly dependent on the parameters to be estimated under the assumption that the observations window contains the non-zero support of the preamble received from each user. In fact, in this case the first contribution in the right hand side (RHS) of (41)

$$C_1=\sum_{i=1}^{U}|c_i|^2\sum_{m=0}^{\eta M-1}\left|\tilde{z}_i^{\tilde{\tau}_i}\left(mT_s\right)\right|^2 \tag{42}$$

is independent of the phase offset and slightly dependent of the symbol timing, while the second term in the RHS of (41)

$$C_2=2\,\mathrm{Re}\left\{\sum_{i_1=1}^{U}\sum_{i_2=1}^{U-i_1}\sum_{m=0}^{\eta M-1}|c_{i_1}||c_{(i_1+i_2)}|e^{j(\tilde{\phi}_{i_1}-\tilde{\phi}_{(i_1+i_2)})}\tilde{z}_{i_1}^{\tilde{\tau}_{i_1}}(mT_s)\tilde{z}_{(i_1+i_2)}^{\tilde{\tau}_{(i_1+i_2)}}(mT_s)^*\right\} \tag{43}$$

related to the scalar product between the signal of the different users, is negligible since the spectra of these signals essentially don't overlap. By substituting (38) in (40) we get

$$\hat{\varphi}_{i_{ML}}=\frac{1}{2\pi}\angle\left\{\gamma\left(\tilde{\tau}_i\right)\right\},i=1,...,U, \tag{44}$$

and, moreover,

$$\hat{\tau}_{i_{ML}}=\arg\max_{\tilde{\tau}_i}\left[\left|\gamma(\tilde{\tau}_i)\right|\right],\qquad i=1,...,U. \tag{45}$$

where

$$\gamma(\tilde{\tau}_i)=\sum_{k=0}^{\eta M-1}r(mT_s)\tilde{z}_i^{\tilde{\tau}_i}(mT_s)^*. \tag{46}$$

Performance evaluation

The performance the proposed ML estimator is assessed via computer simulations. A number of 10^2 Monte Carlo trials has been performed under the following conditions:

- The value of the carrier phase and of the timing offset are uniformly distributed in $[-\pi, \pi)$ and $T_s\{-M/2,M/2\}$, respectively. In particular, the symbol timing is supposed to be an integer multiple of the sampling period T_s.
- The size of the set of subcarriers is M=1024 while the number of users is U=4 and $M_u^i=256$ $i = 1,\ldots,4$ indicates the number of subcarriers per user.
- Three different kinds of allocation schemes, blockwise, interleaved and interleaved b, are considered. In the blockwise scheme, a block of $M_u^i=256$ $i = 1,\ldots,4$ adjacent subcarriers is assigned to the ith user. On the contrary in the interleaved and interleaved b schemes, group of adjacent subcarriers are allocated to different users and in particular, in the former case, one subchannel is dropped between two users (see Figure 4-6).
- The preamble is made up of $N_{TR} = 2$ OFDM/OQAM symbols.
- The prototype filter is that described in Section 2 with an overlapping factor K=4.
- Numerical results have been obtained by considering two different scenarios: AWGN channel and multipath channel modeled using the Vehicular-A channel model of ITU-R. Moreover, the channel is fixed in each run but it is independent from one run to another.

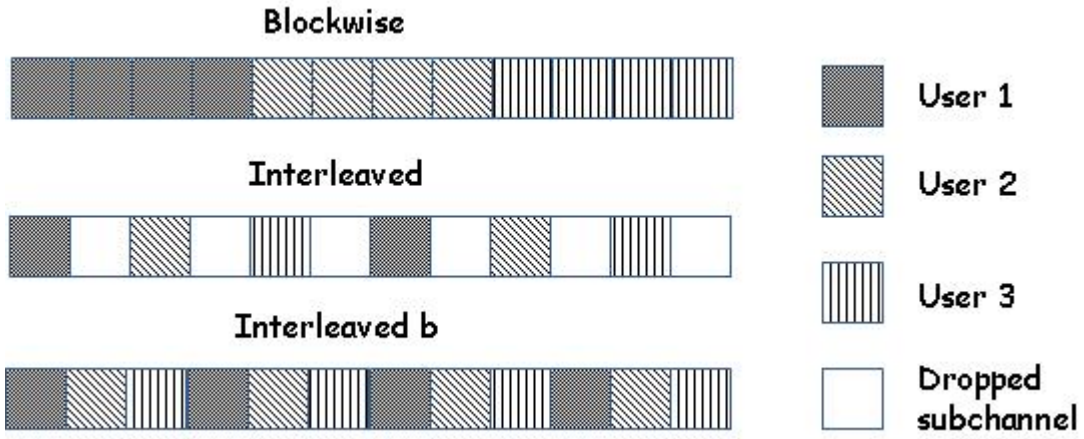

Figure 4-6. Allocation schemes.

In Figure 4-7 we report the behavior of the cost function of the symbol timing ML estimator of the first user in AWGN. The first user is assumed to have an SNR equal to SNR=10dB, while the other users have the same SNR, fixed at SNR=20dB. The results show that the behavior of the cost function is dependent on the adopted allocation scheme, in particular in the cases of interleaved and interleaved b allocation schemes the cost function presents local maxima that can interfere with the absolute maximum especially for low SNR or in multipath channel while in case of blockwise allocation scheme the considered ML cost function exhibits an unique sharp peak at the actual value of the symbol timing.

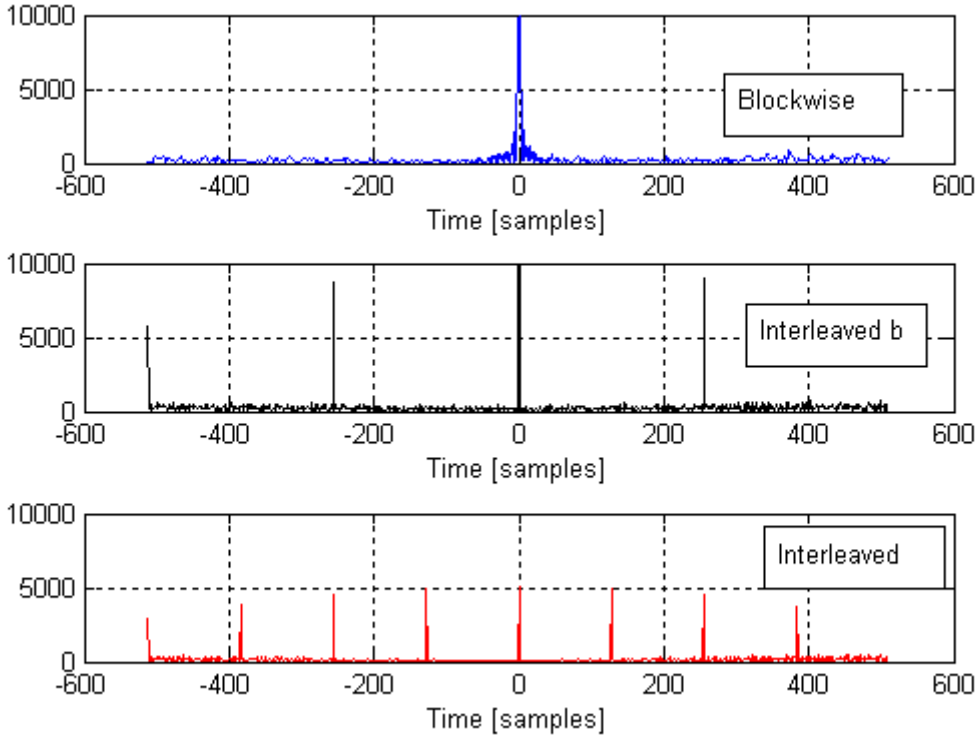

Figure 4-7. Cost function of the proposed ML symbol timing estimator in AWGN for M=1024 and N_{TR} =2.

In Figure 4-8 it is shown the performance of the proposed estimator as a function of the signal-to-noise ratio of the first user in AWGN (solid lines) and multipath channel (dashed lines). The other users are assumed to have the same SNR, fixed at SNR=20dB. The results show that in AWGN and multipath channel blockwise assignment provides the best performance and only for high values of SNR its estimates are comparable with those achieved with the interleaved b and interleaved schemes.

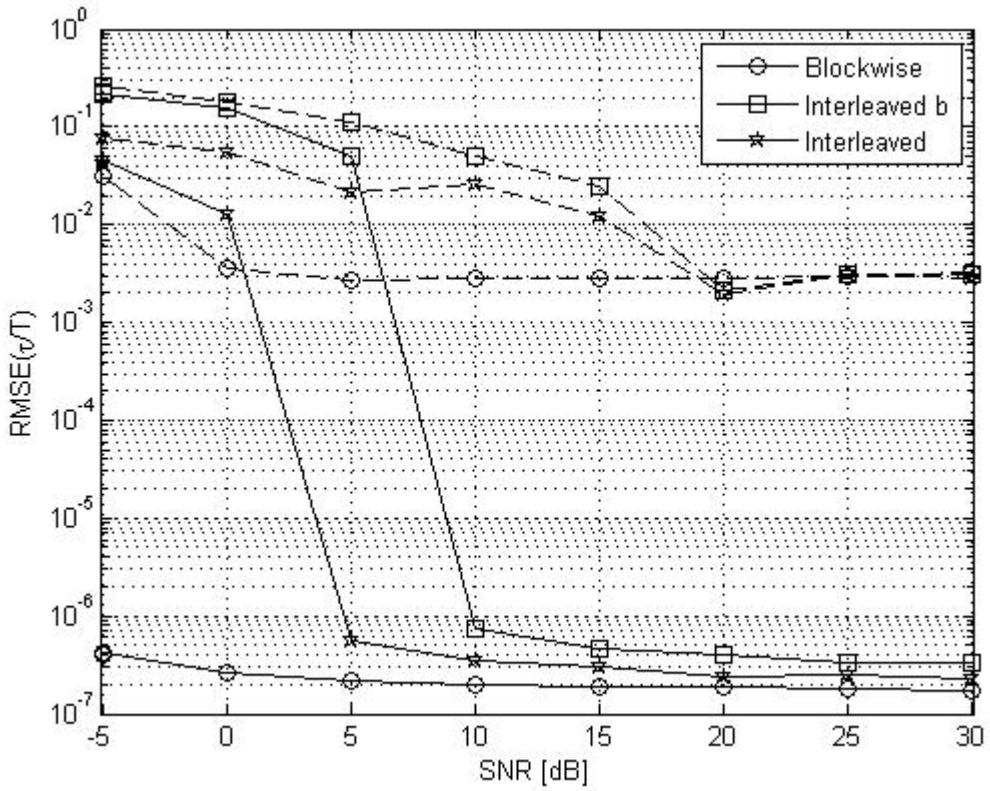

Figure 4-8. Performance of the proposed ML estimator in AWGN and multipath channel as a function of SNR of the first user, for M=1024 and N_{TR} =2.

4.2.2 ML CFO estimator

By following the same steps as in section ML symbol timing estimator4.2.1, we derive the ML CFO estimator for the uplink of an OFDM/OQAM system with perfect symbol timing synchronization. In particular, let us consider a preamble of N_{TR} OFDM/OQAM symbols, the received sequence in AWGN channel and in the presence for each user of a CFO ε_i, a carrier phase offset ϕ_i and an attenuation $|c_i|$, can be expressed as

$$r(mT_s) = \sum_{i=1}^{U} e^{j2\pi\left(\frac{\varepsilon_i m}{M}+\phi_i\right)} |c_i| z_i(mT_s) + n(mT_s) \tag{47}$$

where $z_i(mT_s)$ is the transmitted training sequence defined in (35) while $n(mT_s)$ is the AWGN noise. The likelihood function in AWGN channel for the unknown parameters ε_i and φ_i, $i = 1,...,U$ is given by (up to an irrelevant multiplicative factor)

$$\Lambda\left(\underline{\varepsilon},\underline{\varphi}\right) = \exp\left\{-\frac{T_s}{N_0}\sum_{m=0}^{\eta M-1}\left|r(mT_s) - \sum_{i=1}^{U}|c_i| e^{j2\pi\tilde{\varphi}_i} e^{j\frac{2\pi}{M}\tilde{\varepsilon}_i m} z_i(mT_s)\right|^2\right\} \tag{48}$$

where $\underline{\varepsilon} = (\varepsilon_1, \varepsilon_2, ..., \varepsilon_U)$ and $\underline{\varphi} = (\varphi_1, \varphi_2, ..., \varphi_U)$. After simple algebraic manipulations and dropping irrelevant multiplicative and additive factors we get [2]

$$\ln \Lambda\left(\underline{\varepsilon},\underline{\varphi}\right) = \sum_{i=1}^{U} \mathrm{Re}\left[Z_i\left(\tilde{\varphi}_i, \tilde{\varepsilon}_i\right)\right] \tag{49}$$

where

$$Z_i\left(\tilde{\varphi}_i, \tilde{\varepsilon}_i\right) = |c_i| e^{-j2\pi\tilde{\varphi}_i} \sum_{m=0}^{\eta M-1} r(mT_s) z_i(mT_s)^* e^{-j\frac{2\pi}{M}\tilde{\varepsilon}_i m}. \tag{50}$$

By substituting the expression of the transmitted signal (35) in (50), we get

$$Z_i\left(\tilde{\varphi}_i, \tilde{\varepsilon}_i\right) = |c_i| e^{-j2\pi\tilde{\varphi}_i} \sum_{m=0}^{\eta M-1} r(mT_s) e^{-j\frac{2\pi}{M}\tilde{\varepsilon}_i m} \left(\sum_{k\in M_u^{\,i}} \sum_{n=0}^{2N_{TR}-1} d_{k,n}\theta_{k,n}\beta_{k,n} p\left(mT_s - nT/2\right) e^{j\frac{2\pi}{M}km}\right)^* \tag{51}$$

Hence, (51) becomes

$$Z_i(\tilde{\varphi}_i, \tilde{\varepsilon}_i) = |c_i| e^{-j2\pi\tilde{\varphi}_i} \gamma(\tilde{\varepsilon}_i) \tag{52}$$

where

$$\gamma\left(\tilde{\varepsilon}_i\right) = \sum_{k\in M_u^{\,i}} \sum_{n=0}^{2N_{TR}-1} d_{k,n}\theta_{k,n}^{\,*}\beta_{k,n}^{\,*} w_n^{(k)}\left(\tilde{\varepsilon}_i\right) \tag{53}$$

with

$$w_n^{(k)}\left(\tilde{\varepsilon}_i\right) = \sum_{m=0}^{\eta M-1} r(mT_s) p\left(mT_s - nT/2\right) e^{-j\frac{2\pi}{M}(k+\tilde{\varepsilon}_i)m}. \tag{54}$$

[2] Note that observations similar to those reported in section 4.2.1, after (40), leads to the conclusion that the term $\sum_{m=0}^{\eta M-1}\left|\sum_{i=1}^{U}|c_i| e^{j2\pi\tilde{\phi}_i} e^{j\frac{2\pi}{M}\tilde{\varepsilon}_i m} z_i(mT_s)\right|^2$ is weakly dependent on the parameter to be estimated.

From (49) and (50), it immediately follows that the joint ML estimator for the problem at the hand is

$$\hat{\varphi}_{i_{ML}} = \frac{1}{2\pi}\angle\left\{\gamma\left(\tilde{\varepsilon}_i\right)\right\}, \quad i = 1,...,U, \tag{55}$$

$$\hat{\varepsilon}_{i_{ML}} = \arg\max_{\tilde{\varepsilon}_i}\left[\left|\gamma(\tilde{\varepsilon}_i)\right|\right], \quad i = 1,...,U. \tag{56}$$

Note that if the i-th CFO is sufficiently small that within a time ΔQ comparable with the length of the prototype filter $e^{-j\frac{2\pi}{M}\tilde{\varepsilon}_i\Delta Q} \simeq 1$ it follows that

$$w_n^{(k)}\left(\tilde{\varepsilon}_i\right) \simeq e^{-j\pi\tilde{\varepsilon}_i n} w_n^{(k)}\left(0\right) = e^{-j\pi\tilde{\varepsilon}_i n}\sum_{m=0}^{\eta M-1} r(mT_s)e^{-j\frac{2\pi}{M}mk}\, p(mT_s - nT/2) \tag{57}$$

Therefore, the ML estimator can be simplified as

$$\hat{\varphi}_{i_{AML}} = \frac{1}{2\pi}\angle\left\{\gamma\left(\tilde{\varepsilon}_i\right)\right\}, \quad i = 1,...,U \tag{58}$$

$$\hat{\varepsilon}_{i_{AML}} = \arg\max_{\tilde{\varepsilon}_i}\left[\left|\gamma(\tilde{\varepsilon}_i)\right|\right], \quad i = 1,...,U \tag{59}$$

where

$$\gamma\left(\tilde{\varepsilon}_i\right) = \sum_{k\in M_u^{\,i}}\sum_{n=0}^{2N_{TR}-1} d_{k,n}\theta_{k,n}{}^{*}\beta_{k,n}{}^{*} w_n^{(k)}\left(0\right)e^{-j\pi\tilde{\varepsilon}_i n}.$$

Performance evaluation

The performance the proposed ML and AML estimators is assessed via computer simulations. A number of 10^2 Monte Carlo trials has been performed under the following conditions:

- The value of the carrier phases is uniformly distributed in [-π, π) while the CFO values are fixed at [0.01, 0.02, 0, 0.05].
- The size of the set of subcarriers is M=1024 while the number of users is U=4 and M_u^i=256 i = 1,…,4 indicates the number of subcarriers per user.
- Three different kinds of allocation schemes, blockwise, interleaved and interleaved b, are considered (see Figure 4-6).
- The preamble is made up of N_{TR} = 2 OFDM/OQAM symbols.
- The prototype filter is that described in Section 2 with an overlapping factor K=4.

In Figure 4-9 is reported the behavior of the cost function of the ML and AML CFO estimators for the first user in AWGN. The first user is assumed to have an SNR equal to SNR=10dB, while the other users have the same SNR, fixed at SNR=20dB. The results show in the all considered cases the ML and AML cost functions present a maximum at the actual value of the CFO ε_l=0.

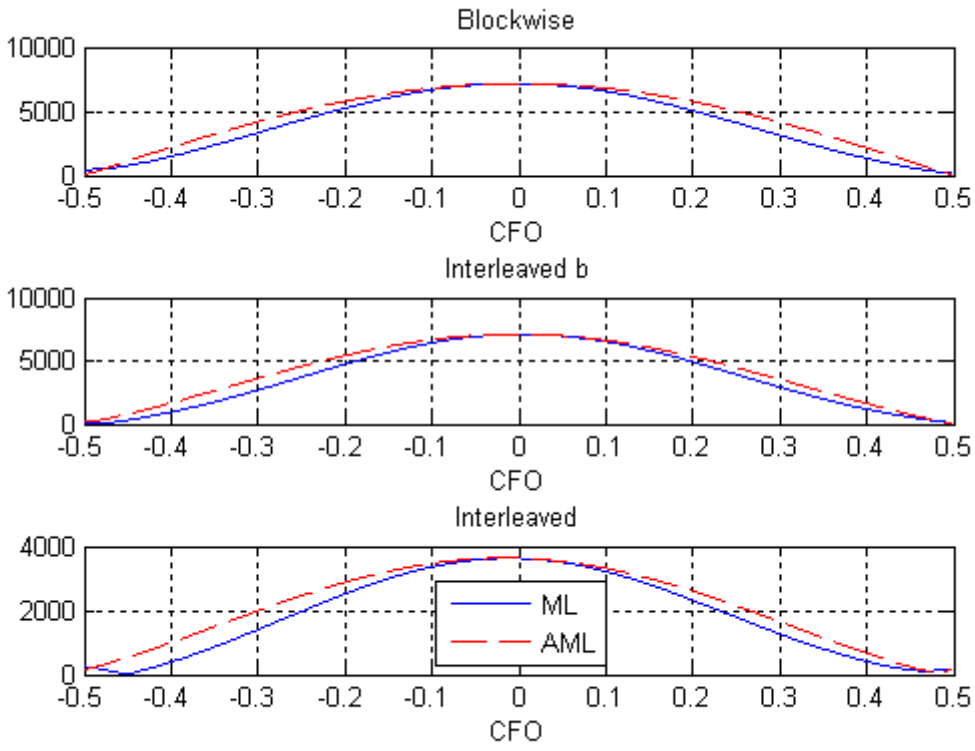

Figure 4-9. Cost function of the proposed CFO estimators in AWGN for M=1024 and N_{TR} =2.

In Figure 4-10 it is shown the performance of the proposed ML and AML estimators as a function of the signal-to-noise ratio of the first user in AWGN. The other users are assumed to have the same SNR, fixed at SNR=20dB. The results show that the estimators in the blockwise and interleaved b cases provide nearly the same performance for all considered SNR values.

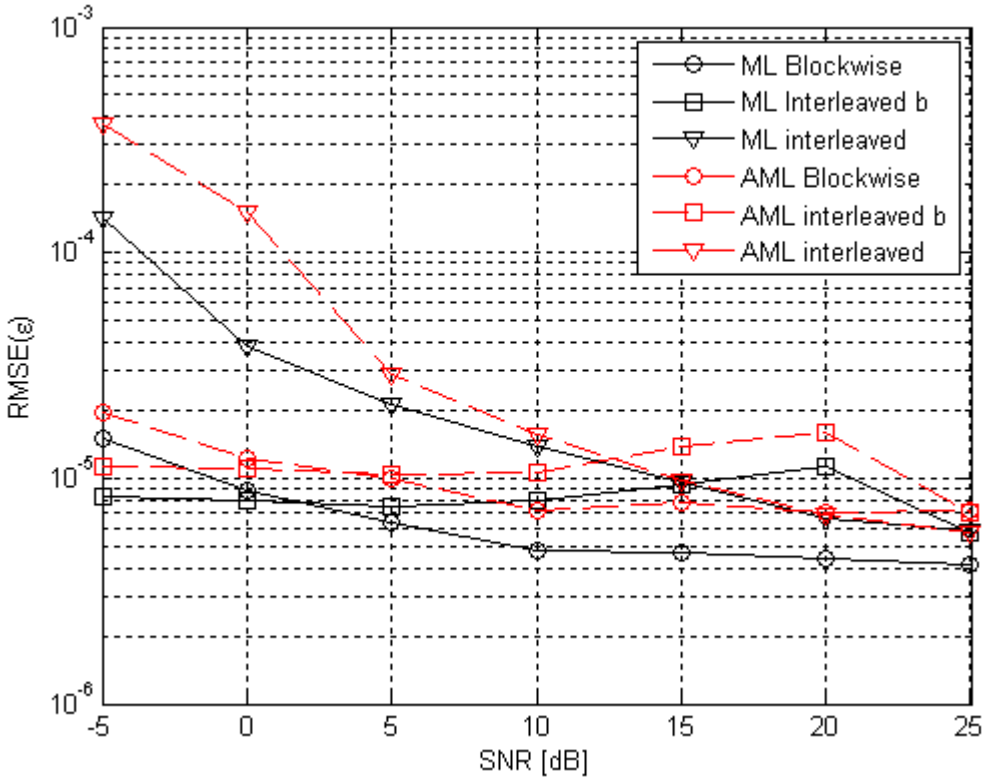

Figure 4-10. Performance of the considered CFO estimators in AWGN for M=1024 and N_{TR} =2.

5 Pilot-based CFO and symbol timing schemes

In multicarrier literature, pilots refer to known training symbols which are scattered among data symbols at predetermined subcarrier symbol positions, following patterns which are characteristic to each particular system. Due to the use of OQAM subcarrier modulation, the use of pilots in FBMC systems is not as straightforward as in OFDM. Two different pilot schemes have been presented in [13] and [14] for channel estimation purposes. However, to the best of our knowledge, pilot-based CFO or timing estimation methods have not been presented in the literature so far.

We utilize here the idea of [13] to construct FBMC pilots which can be used basically in the same way as pilots in OFDM. In Section 5.1, this auxiliary pilot scheme is applied with the PHYDYAS reference filter bank and certain simplifications in calculations related to the pilot construction are discussed. In Section 5.2 we discuss possibilities to apply the auxiliary pilot scheme with WiMAX (802.16e) -like pilot patterns. In Sections 5.3 and 5.4, the auxiliary pilot schemes are applied to CFO estimation and symbol timing estimation, respectively.

Both mentioned pilot schemes are investigated in the PHYDYAS deliverable D3.1 [7] in the channel estimation context, considering also the joint effects of synchronization and channel estimation. The possibilities to use the interference estimation based approach of [14] for the synchronization tasks remains as a topic for future studies.

5.1 Auxiliary pilot scheme

In an OQAM-FBMC system, either real or imaginary parts of the complex subcarrier symbols are used for data transmission in a staggered fashion. As discussed in Section 2.4, when a real (imaginary) part of a subcarrier symbol is used, the unused imaginary (real) part is, at the receiver, a fairly complicated function of surrounding data symbols. In the following, we refer to these two parts of the complex symbols as primary and secondary parts, respectively. In the case of PR filter bank system, there is no crosstalk among the primary parts (or secondary parts) themselves. In the case of near NPR filter banks, like the PHYDYAS reference bank, the crosstalk effects between the primary parts are small enough to be neglected.

The nature of FBMC systems makes it impossible to construct pilot symbols for channel estimation and synchronization purposes in the same way as in OFDM. The approach taken in [13] is based on the observation that it is enough to select one of the subcarrier symbols close to a pilot symbol as an associated auxiliary pilot. Adjusting the primary part of the auxiliary pilot depending on the surrounding data symbols, the secondary part of the actual pilot can be forced to take any desired value. For example, the secondary part of the complex pilot symbol can be forced to zero. Utilizing this idea, pilots can be used in FBMC systems in a similar way as in OFDM. It should be noticed that the relative pilot overhead using this idea is the same as the pilot overhead in OFDM, i.e., for each pilot, one OQAM symbol is used in the FBMC case and one QAM symbol in the OFDM case. However, in the presented auxiliary pilot scheme, there are several alternatives in choosing the location of the auxiliary pilot. It is not necessary to place the pilot and auxiliary pilot in the same OQAM symbol.

In case of a frequency-selective channel and sufficiently narrow subcarrier spacing, the pilot would suffer from attenuation and phase rotation directly related to the channel. Simple estimation of the

received pilot amplitude and phase yields estimates for the channel's amplitude and phase for that frequency bin.

Based on Section 2.4, looking at the AFB output samples in the receiver in case of an ideal channel, the symbol (pilot) of interest at (k_p, n_p), can be expressed as:

$$x_{k_p,n_p} = \sum_{(k,n)\in\Omega_{k_p,n_p}} d_{k,n}\theta_{k,n}t_{k_p-k,n_p-n}\ , \tag{60}$$

where Ω_{k_p,n_p} is the set of neighboring symbol positions which have a significant effect on the symbol at (k_p, n_p). Especially, the secondary part of the symbol is

$$u_{k_p,n_p} = \sum_{(k,n)\in\Omega_{k_p,n_p}} d_{k,n}\,\mathrm{Im}\left[\theta_{k-k_p,n-n_p}t_{k_p-k,n_p-n}\right] = \sum_{(k,n)\in\Omega_{k_p,n_p}} d_{k,n}\hat{t}_{k_p-k,n_p-n}\ , \tag{61}$$

where

$$\hat{t}_{k,n} = \mathrm{Im}\left[(-j)^{k,n}t_{k,n}\right], \tag{62}$$

whereas the primary part is the original primary value, d_{k_p,n_p}, plus some additive interference which can be assumed to be negligible.

The transmultiplexer response $t_{k,n}$ is known from the filter bank design. If the prototype filter is designed with good frequency selectivity and roll-of factor $\alpha \le 1$, the range includes k_p and both adjacent subcarriers, $k_p - 1$ and $k_p + 1$ in the frequency dimension. The range of *n* is [*n*-*K*, *n*+*K*], e.g., 7 or 9 subcarrier samples with the typical overlapping factors (*K*) of 3 or 4.

The auxiliary pilot position is denoted in the following as (k_a, n_a) and the auxiliary pilot is assumed to be chosen in such a way that the secondary part of the pilot sample becomes zero. This can be achieved by choosing

$$d_{k_a,n_a} = -\frac{\sum_{\substack{(k,n)\in\Omega_{k_p,n_p}\\(k,n)\neq(k_p,n_p)\\(k,n)\neq(k_a,n_a)}} d_{k,n}\hat{t}_{k_p-k,n_p-n}}{\hat{t}_{k_p-k_a,n_p-n_a}} \tag{63}$$

We notice that a small absolute value of $\hat{t}_{k_p-k_a,n_p-n_a}$ results in large magnitude of the auxiliary pilot, which wastes transmission energy and is expected to be bad for the peak-to-average power ratio (PAPR) of the transmitted waveform. Thus it is preferable to choose the auxiliary pilot in such a way that the magnitude of the denominator is maximized. In typical filter bank designs, including the Phydyas reference filter bank, the choice for the auxiliary pilot is the sample immediately preceeding or following the pilot, i.e., $(k_p, n_p - 1)$ or $(k_p, n_p + 1)$.

Performance evaluation

Figure 5-1 shows two alternative definitions for the Ω_{k_p,n_p} . The smaller window includes 11 subcarrier samples (excluding the pilot and auxiliary pilot) and the larger one 17 samples. The values of $\hat{t}_{k_p,n_p-1}$ and $\hat{t}_{k_p,n_p+1}$ are equal to 0.5644. This value is about double compared to the second largest magnitude in Ω_{k_p,n_p} .

For the preliminary simulations, we have considered a configuration of one pilot regularly placed in a group of 8 subcarriers. With this configuration, we show simulation based results on the interference and also on the PAPR when the data in the data subcarriers consists of QPSK symbols. The average power level of the auxiliary pilots with this configuration is somewhat higher than 3 dB above the pilot power level.

In case of ideal channel model, the complex residual interference in the pilot values is the joint effect of the use of NPR filter bank and the use of limited widow size in the auxiliary pilot calculations. Figure 5-2 presents the histogram of the amplitude of the residual interference in the case of the wider window. The shape clearly indicates a non-biased Gaussian noise-like distribution. In the case of the narrower window, the distribution is more quantized, but probably higher order modulation would smoothen the shape.

0	-0.0006	-0.0001	0	0	0	-0.0001	0.0006	0
-0.0054	-j.0429	-0.1250	-j.2058	-0.2393	-j.2058	-0.1250	-j.0429	-0.0054
0	-0.0668	-0.0002	-0.5644	**1**	0.5644	-0.0002	0.0668	0
0.0054	-j.0429	0.1250	-j.2058	0.2393	-j.2058	0.1250	-j.0429	0.0054
0	-0.0006	-0.0001	0	0	0	-0.0001	0.0006	0

(a)

0	-0.0006	-0.0001	0	0	0	-0.0001	0.0006	0
-0.0054	-j.0429	-0.1250	-j.2058	-0.2393	-j.2058	-0.1250	-j.0429	-0.0054
0	-0.0668	-0.0002	-0.5644	**1**	0.5644	-0.0002	0.0668	0
0.0054	-j.0429	0.1250	-j.2058	0.2393	-j.2058	0.1250	-j.0429	0.0054
0	-0.0006	-0.0001	0	0	0	-0.0001	0.0006	0

(b)

Figure 5-1. Auxiliary pilot calculation windows for PHYDYAS reference bank. (a) Narrow window. (b) Wider window.

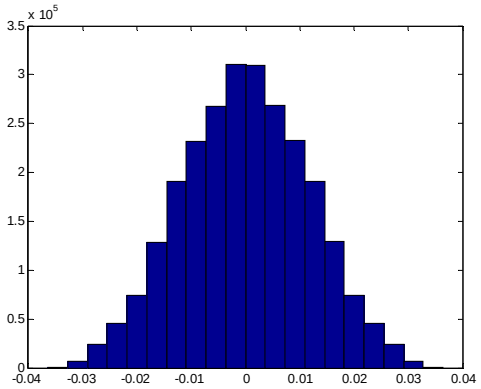

Figure 5-2. Histogram of residual pilot interference with wider window.

Assuming the imaginary noise to be Gaussian, the residual interference is at the level of -17.8 dBr with smaller window and at -38.7 dBr with wider window, considering the real pilot symbol amplitude of 1 as the reference. It is obvious that the wider window should be utilized.

From the peak to average power point of view, the effect of the auxiliary pilot seems moderate, at least in the 10000 realization sets that we performed, as can be seen in Figure 5-3.

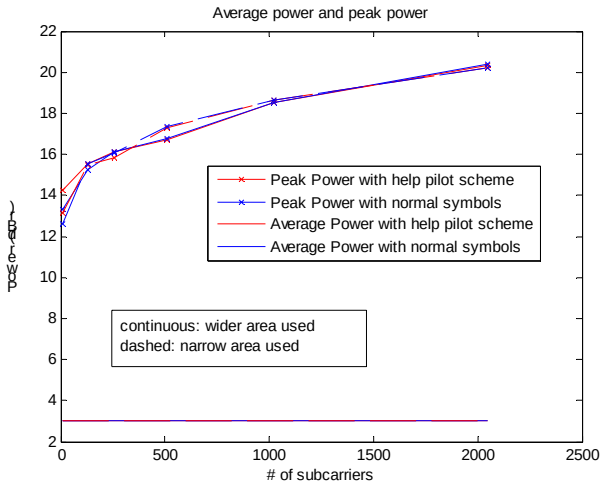

Figure 5-3. Effect of auxiliary pilots on the PAPR with PHYDYAS reference bank.

The performance of the auxiliary pilot scheme in channel estimation is reported in [7]. Also the conclusion from channel estimation performance evaluation is that the wider window provides sufficient performance, as far as the quality of the pilots is considered, but with narrower window, the performance is clearly worse.

5.2 Application of auxiliary pilot scheme to WiMAX pilot structures

The target of Phydyas is to develop a WiMAX-like air-interface using the FBMC approach. Thus it is natural to consider direct adaptation of the 802.16e pilot patterns to the FBMC model.

Let us consider first the pilot structure used in the *adaptive modulation and coding* (AMC23) mode, both in uplink and downlink. The AMC23 OFDM pilot pattern is shown in Figure 5-4(a). Here each OFDM symbol corresponds to two consequtive subcarrier samples in the FBMC model. It can be seen that auxiliary pilot calculations can be done without difficulties using the PHYDYAS reference filter bank and the principles described above. Regular pilot structure can be easily used. The natural choice is to select the auxiliary pilot to be in the same OQAM symbol with the pilot.

In the downlink *partial usage of subchannels* (PUSC) mode, illustrated in Figure 5-4(b), there are some difficulties. If a regular placement of auxiliary pilots is adopted and the wider window is used in the auxiliary pilot calculations, there will be cases where an auxiliary pilot is in the window of another auxiliary pilot. In this case, recursive calculation of auxiliary pilots would be required, which may be somewhat inconvenient. However, by using a slightly modified pilot scheme, this difficulty can be avoided, and each of the auxiliary pilots can be calculated independently of the others. In the modified scheme, the order of pilot and auxiliary pilot is exchanged in every second instance within a subcarrier, as illustrated in Figure 5-5.

The uplink-PUSC (see Figure 5-4(c) is even trickier due to the higher density of pilots. Even with smart positioning of the pilots and help pilots, the calculation of each help pilots requires the solving of a equation system of 4 equations with 4 unknowns. This makes the auxiliary pilot calculations more complicated in the uplink-PUSC mode.

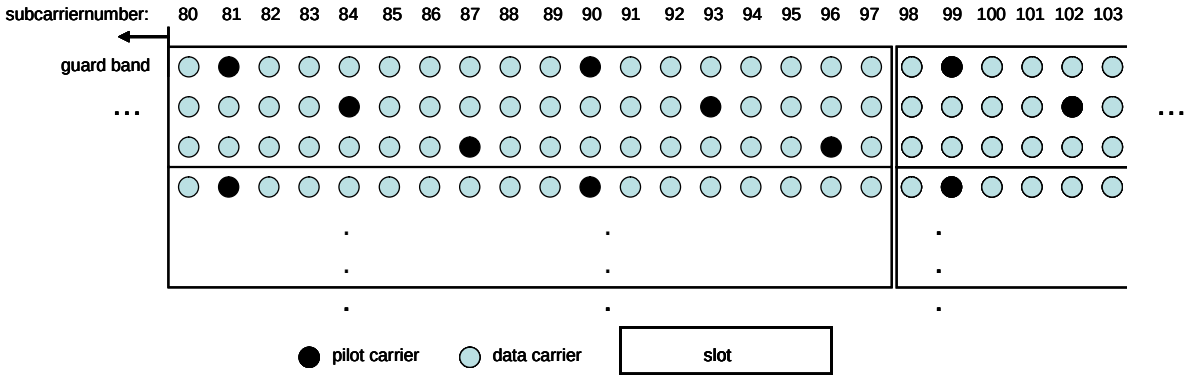

(a)

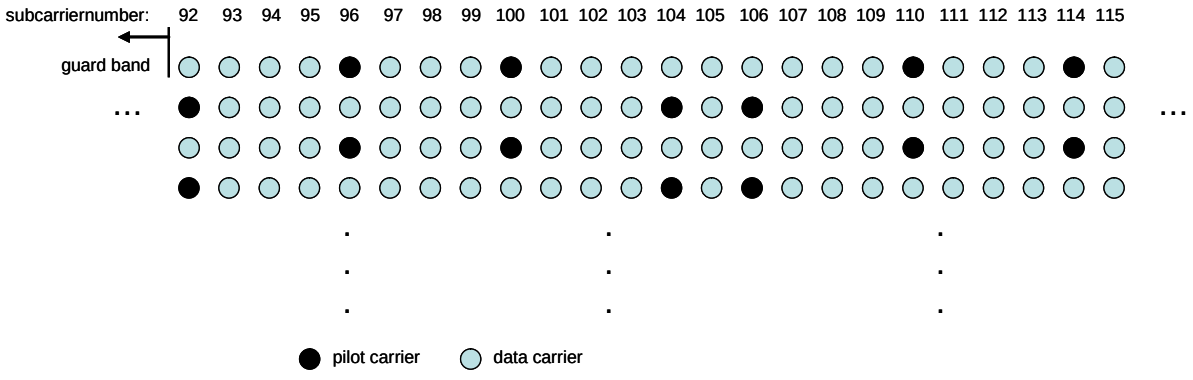

(b)

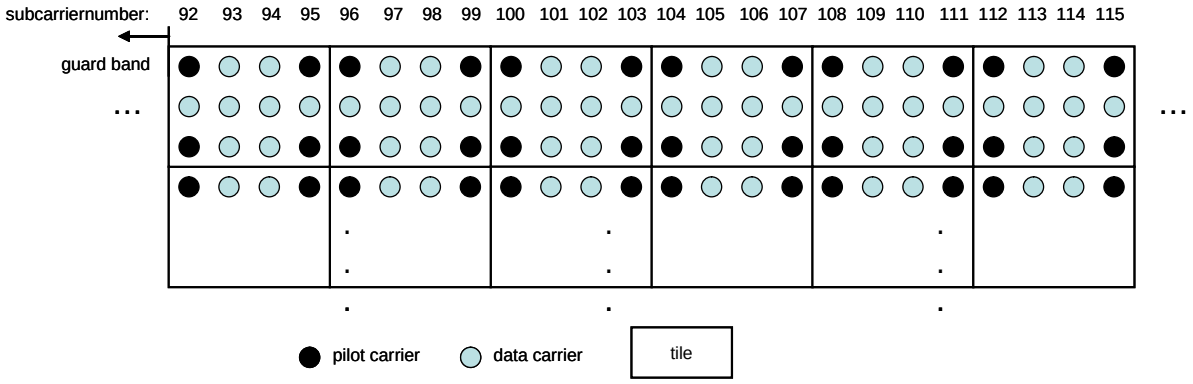

(c)

Figure 5-4. Pilot and data allocations in WiMAX (OFDM). (a) AMC23 (b) DL PUSC (c) UL PUSC

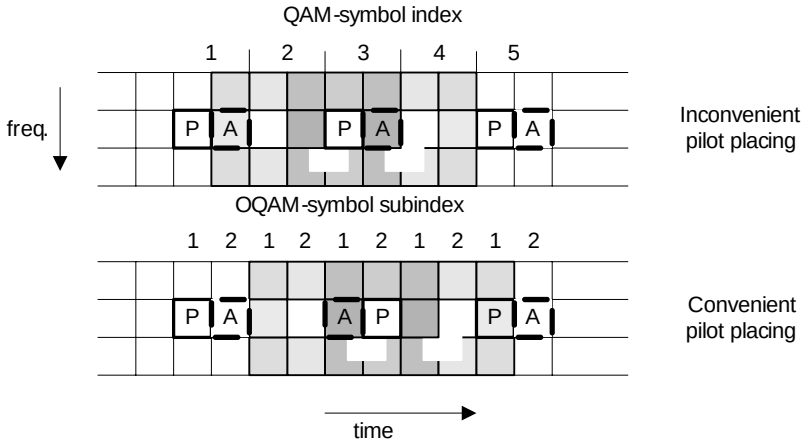

Figure 5-5. Alternative pilot and data allocations for FBMC with DL PUSC like pilot pattern.

5.3 Auxiliary pilot based estimation of CFO

One very basic scheme for estimating the carrier frequency offsets in multicarrier systems is based on measuring the time-varying phase rotation of the pilots. This approach has been used in OFDM systems, e.g., for CFO tracking [15]. In an FBMC system, the phase rotation between two consecutive pilots in the same subcarrier is

$$\Delta\phi = \pi\varepsilon \cdot \Delta n \tag{64}$$

where ε is the carrier frequency offset normalized to subcarrier spacing and Δn is the pilot spacing in terms of subcarrier samples. In the auxiliary pilot scheme, the time-varying rotation of the pilots is the dominant effect with small CFO values. With increasing CFO, inter-carrier interference (ICI) will also be introduced on top of the pilots. In the following discussion, the ICI effect will be ignored. The ICI effect can be reduced by averaging over multiple pilot-based measurements, which naturally helps also against the effecs of channel noise.

In case of CFO together with (quasi-) static frequency selective channel with flat-fading subcarriers, the channel response causes constant phase rotation and attenuation, in addition to the time-varying phase-rotation due to CFO. The time-varying part of the CFO is the same in all subcarriers. To

improve the estimation accuracy, the CFO estimates can be averaged over multiple subcarriers and over consecutive pilot pairs in each subcarrier. Naturally, it is advantageous to choose a sufficient number of the strongest subcarriers for the estimation. The estimate can be written as:

$$\hat{\varepsilon} = \frac{1}{\pi \Delta n} \angle \left(\sum_{(k,n) \in \Omega_{CFO}} \theta^{-\Delta n} y_{k,n+\Delta n} y_{k,n}^{*} \right) \tag{65}$$

where Ω_{CFO} is the set of pilot locations used for CFO estimation and $y_{k,n}$ are received complex subcarrier samples at the pilot locations.

In this scheme, the CFO estimation range is limited to $\left[-\Delta f / \Delta n, \Delta f / \Delta n\right]$, i.e., it depends essentially on the pilot distance in subcarriers. For example, in the AMC mode of 802.16e, the pilot distance in pilot subcarriers is 3 OFDM symbols. Direct adaptation of the pilot structure to FBMC case using the auxiliary pilot scheme leads to the distance of $\Delta n = 6$ subcarrier samples. The corresponding CFO estimation range is $\left[-\Delta f / 6, \Delta f / 6\right]$ or ±1.82 kHz. In the downlink PUSC mode of 802.16e, the pilot distance is 2 OFDM symbols, and in the corresponding FBMC pilot pattern proposed in Section 5.3, the minimum $\Delta n = 3$ and the CFO estimation range is limited to ±3.65 kHz. Of course, with such high CFO values, the ICI will significantly disturb the CFO estimation.

A necessary precondition for this procedure is a constant frequency offset during the transmission of a single packet or within a single frame, respectively. The frequency offset (due to Doppler) changes if the speed of the MS is changing. Thus the acceleration of the MS has to be considered. Let's assume a constant acceleration of a = 2.8 m/s^2 (0 km/h to 100 km/h in 10 seconds) and a 5 ms frame length, as used in 802.16e. Let the actual speed at the beginning of frame be v_1 = 50 km/h, then the Doppler shift is (carrier freq = 2.5 GHz) $\Delta f_1 \approx 115.74$ Hz. At the end of the frame the speed is $v_2 = v_1 + 14 \cdot 10^{-3}$ m/s. Thus the Doppler shift at the end of the frame is $\Delta f_2 \approx 115.86$ Hz. The change of the offset due to the change of Doppler shift from the beginning of a frame to the end is negligible.

Performance evaluation

The auxiliary pilot based CFO estimation method was tested using WiMAX-like parameters:

- FFT-size: 1024
- Bandwidth: 10 MHz
- Subcarrier spacing: 10.94 kHz
- Pilot pattern: evenly-spaced over used subcarriers, every 3rd OQAM symbol consists of pilot and auxiliary pilot in pilot subcarriers (AMC configuration)

The statistics include 100 independent channel realizations for each of 15 different CFO values. These results should be considered preliminary; the study will be repeated with extensive statistics in the near future.

The performance was tested using the Vehicular-A channel model of ITU-R with 5 dB E_b/N_0-ratio and 6 dB pilot boost (overall boost for pilot and auxiliary pilot), including also a timing offset of 5 % of the OQAM symbol length. The results are shown in Table 5-1 with different pilot configurations. It can be seen that this method is quite robust, providing good performance with

modest number of pilots and in the presence of multipath channel and significant timing offset. In the simulations, it was observed that the RMS and maximum estimation error doesn't significantly depend on the CFO value. However, close to the end of the estimation range, occasional outliers degrade the estimation performance, when the number of pilots used for estimation is low.

In this example, the pilot spacing in the time domain corresponds here to the AMC pattern of WiMAX. With sufficient number of pilots, it is possible to approach the theoretical estimation range $(-\Delta f/6, \Delta f/6)$ quite well. In preliminary tests, also in the PUSC case with the modifed auxiliary pilot scheme, it is possible to approach the theoretical estimation range of $(-\Delta f/3, \Delta f/3)$. It might be interesting to consider even smaller pilot spacings in order to extend the estimation range. Using the auxiliary pilot scheme, it is even possible to locate two pilots next to each other (aux pilot 1 – pilot 1 – pilot 2 – aux pilot 2) within a subcarrier, in which case $\Delta n = 1$.

Table 5-1. CFO estimation error for different pilot configurations for Vehicular-A channel, E_b/N_0=5 dB, 6 dB pilot boost, timing offset 5% of OQAM interval. Estimation errors normalized to subcarrier spacing Δf

Number of pilots Time x frequency	Normalized RMS error	Normalized maximum error	Reliable estimation range
2 x 8	0.0094	0.045	(-0.13, 0.13)
3 x 8	0.0047	0.020	(-0.15, 0.15)
4 x 8	0.0035	0.019	(-0.15, 0.15)
2 x 16	0.0069	0.028	(-0.15, 0.15)
3 x 16	0.0033	0.013	(-0.15, 0.15)
4 x 16	0.0027	0.012	(-0.15, 0.15)
2 x 32	0.0047	0.020	(-0.15, 0.15)
3 x 32	0.0019	0.012	(-0.16, 0.16)
4 x 32	0.0017	0.0074	(-0.16, 0.16)

The CFO compensation results presented in Chapter 5.6 of [7] are based on a similar averaging over the strongest subcarriers, but using linear regression to calculate the phase slope. This approach becomes handy when having varying Δn, as for example in the DL-PUSC pilot configuration that is shown in the lower part of Figure 5-5.

5.4 Auxiliary pilot based estimation of timing offset

Timing offset introduces a linearly frequency-dependant phase slope. One basic difficulty in pilot-based estimation of timing offset is that, in case of significant timing offset, the subchannels cannot be expected to be flat-fading anymore, and the quality of basic pilot-based estimation degrades. One possibility for estimating small timing offset is to use least-squares match of linear phase response to the subcarrier-wise channel estimates obtained through the auxiliary pilots. However, this approach has turned out to have rather limited performance.

Here we consider a completely different approach which is closely related to channel estimation and equalization. This approach utilizes the frequency selectivity introduced by the linear phase slope within each pilot subcarrier. We assume a simplified signal model, where the amplitude response is assumed to be constant within each subcarrier and the phase is assumed to be a linear function of

frequency. We consider using a three-tap frequency-sampling based subcarrier equalizer, which is shown in [7] to perform fairly well in channel equalization, also in the presence of modest timing offsets. In [7], the channel estimation is separated into two parts: estimation of the complex channel coefficient for each subcarrier, and estimation of the phase slope jointly for all subcarriers. Assuming that the phase slope is known, the channel coefficients can be easily calculated from the pilots. On the other hand, if the channel coefficients are known, the phase slope can be estimated analytically by minimizing the least-squares error between the known pilots and the equalized received sample values. Solving these two parts of the problem iteratively has been found out to converge to the optimum solution, typically in 2-5 iterations.

The timing offset estimation is important in FBMC systems for two reasons:

1. It is one efficent way to enhance the basic pilot-based channel estimation methods (which are suitable to essentially flat-fading subcarriers only) in case of modest timing offset (e.g., up to 5 % of OQAM symbol interval in case of 64-OQAM modulation).
2. Timing estimation is needed in TDD/FDMA schemes to approximatively synchronize the signals of different uplink users at the base-station receiver. This is achieved by sending timing adjustment feedback information to the mobile station.

It should be noticed that in case of a fading multipath channel, very precise symbol timing estimation cannot be expected, and some guard interval is anyway need in the uplink synchronization. Actually, the FBMC system is more relaxed in this respect compared to OFDM. In OFDM, the sum of channel delay spread and timing offset should be within the guard interval to maintain orthogonality. In the FBMC case, the orthogonality is achieved through an unused subchannel between different asynchronous users, and timing is not critical. The worst case timing offset has anyway an effect on dimensioning of the transition intervals between downlink and uplink transmissions.

Performance evaluation

The auxiliary pilot based timing offset estimation was tested using the same WiMAX-like parameters and simulation scenario as described in the CFO studies in Section 5.3. Using 32 equally-spaced pilot subcarriers, 3 pilots in each subcarrier with spacing of 6 subcarrier samples, the following RMS estimation errors were obtained (τ is the timing offset normalized to the OQAM symbol interval and τ_{RMS} is the maximum RMS error, the reference being the first channel tap):

- AWGN channel with 5 dB E_b/N_0 ratio and 6 dB pilot boost:
  - $\tau_{RMS} < 0.013$ (13 samples) when $\tau<0.1$
  - $\tau_{RMS} < 0.020$ (20 samples) when $\tau<0.5$
- Multipath channel (Veh-A) with 5 dB E_b/N_0 ratio and 6 dB pilot boost:
  - $\tau_{RMS} < 0.017$ (17 samples) when $\tau<0.1$
  - $\tau_{RMS} < 0.022$ (22 samples) when $\tau<0.5$

In conclusion, the proposed timing estimation method seems to provide satisfactory performance for FBMC systems. However, the timing estimation performance seems to be much more sensitive to the number of pilots used in the estimation than the CFO estimation method of Section 5.3.

6 Transmission burst shaping and filter bank memory pre-loading techniques

In this chapter, memory pre-loading and the resulting transmission burst truncation in filter bank based multicarrier modulation are discussed. In particular, the effects of shortening the burst generated in the transmitter are evaluated. The shortening is done by cutting off parts both in the beginning and at the end of the burst (named as pre-tail and post-tail, respectively). The impact of truncation is evaluated in terms of mean-squared error in symbol detection, out-of-band leakage and bandwidth efficiency. This is a topic of great importance when overheads in time are to be minimized in order to maximize the spectral efficiency of the FBMC modulation.

The chapter is organized as follows. In the first section, the burst formatting model is described. In Section 6.2, the principle of filter bank pre-loading is presented. Section 6.3 describes a weighting window model for the pre-loading -induced burst truncation. Moreover, the relations of the weighting window (truncation) parameters and the level of resulting degradation in symbol detection and out-of-band leakage are analyzed. The optimization of the FBMC burst truncation (or equivalently the pre-loading) is discussed in Section 6.4. In Section 6.5, the spectral efficiency of the FBMC transmission with burst truncation is discussed.

6.1 Signal model

Figure 6-1 shows a burst consisting of $N_s = 6$ OQAM symbols ($n = 0,1,\ldots,2N_s - 1$) synthesized using the PHYDYAS reference filter bank with $M = 512$ and overlapping factor $K = 4$. Although being a simplified representation compared to the overall multicarrier multiplex (Figure 6-1 shows the contribution of a single subcarrier only), the information relevant for the following analysis is visible. The length of the synthesized burst in samples $L_B = 2L_T + L_D$, where $L_T = (K-1)\frac{M}{2} + \frac{M}{4}$ and $L_D = N_s M$ denote the length of the tails and the body of the burst, respectively. Note that L_D corresponds to the length of the conventional OFDM/QAM burst carrying N_s QAM symbols, when the cyclic prefix overhead is not considered. Clearly, the length of the pre- and post-tail of the burst depends on the filter bank design through the number of subchannels M and the overlapping factor K. In order to achieve highly frequency selective subchannels, the major property distinguishing FBMC modulation from conventional multicarrier schemes, prototype filters with $K \geq 3$ are typically considered. This means that the tails of the transmitted burst can have significant duration. On the other hand, the length of the tails has a direct impact on how closely different bursts can be placed in time with respect to each other. Therefore, the tails of the FBMC burst influence the achievable spectral efficiency by introducing time domain overhead during transitions between the uplink and downlink transmission modes in time-division duplexing (TDD) based systems and possibly also between different time-division multiplexed uplink users. In the forthcoming analysis, the feasibility of truncating the burst by reducing the effective duration of the tails in the transmitter is studied. The objective is to minimize the required overheads in time, while taking into account the distortion introduced by such processing.

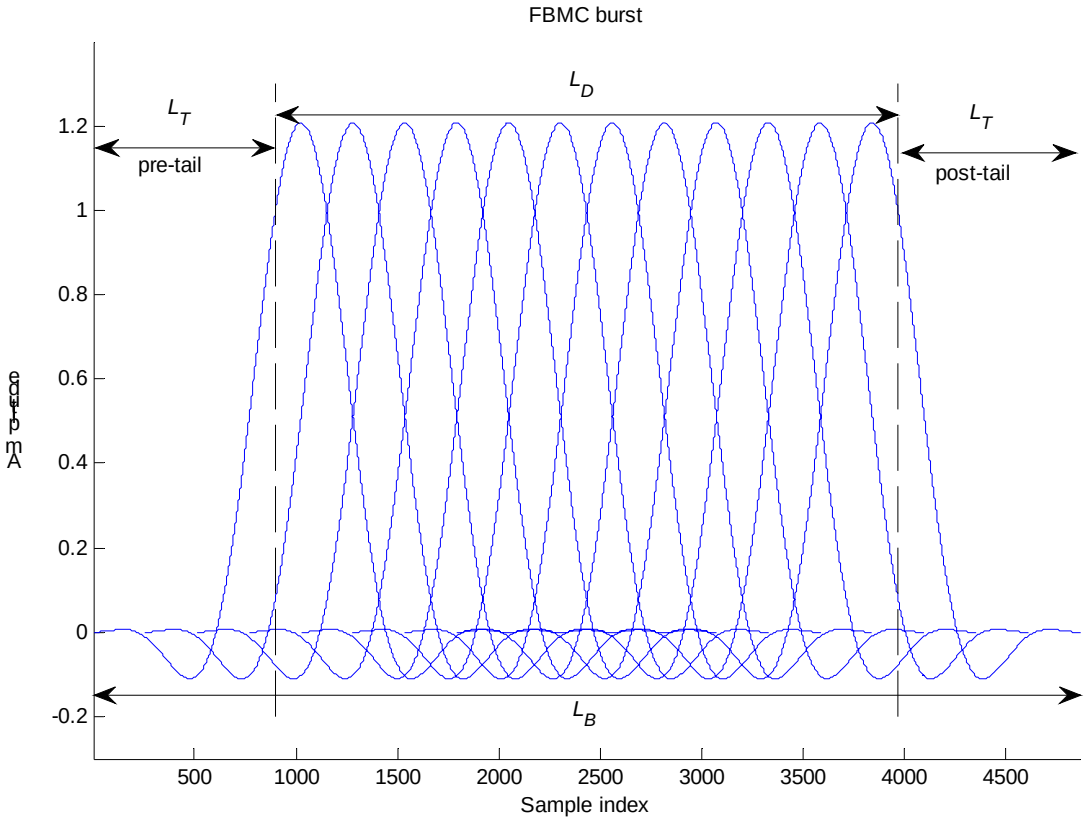

Figure 6-1. An example of FBMC burst carrying $N_s = 6$ OQAM symbols ($M = 512$, $K = 4$).

6.2 Filter bank pre-loading

The one single feature dominantly characterizing filter bank based transmission is its impulse response which extends over multiple consecutive symbol intervals. In order to guarantee maximum utilization of the assigned/available temporal resources, the delay introduced by the polyphase filtering (see Section 2.3 for clarification) in the synthesis bank should be minimized. The effective delay can be reduced by a technique called filter bank memory pre-loading. In pre-loading, instead of initializing the polyphase filtering with zero-filled registers, the IFFT transformed data is pre-loaded into the delay lines of the polyphase branch filters, corresponding to the first desired output sample, prior initiation of the filtering. Memory pre-loading therefore beneficially allows transmission of data in earliest possible time instant by reducing the length of the burst tails, processing referred hereafter as burst truncation. This increases the spectral efficiency of FBMC transmission by minimizing the required overhead in time induced by the tails of the synthesized bursts. However, burst truncation unavoidably results in reduction of the effective impulse response length of the first (pre-tail) and last (post-tail) symbols of the FBMC burst, causing distortion during the corresponding symbols. The following sections analyze the tradeoff between the level of distortion introduced by such burst tail truncation and the obtainable improvement in spectral efficiency.

6.3 Burst truncation

The burst truncation induced by the pre-loading can straightforwardly be modeled using a rectangular weighting window with a 'zeroes - ones - zeroes' weight pattern. In order to generalize the analysis, also smoother weighting windows can be considered. A natural choice is a window with raised cosine (RC) shaped transitions between zero and unity weights, because it can be designed in such a way that it does not affect the body of the burst. It can be described as follows:

$$w[m]=\begin{cases} 0 & \text{for } 0 \le m < b_1 \\ \frac{1}{2}+\frac{1}{2}\cos\left(\pi+\frac{(m-L_z)\pi}{L_w-1}\right) & \text{for } b_1 \le m < b_2 \\ 1 & \text{for } b_2 \le m < b_3 \\ \frac{1}{2}+\frac{1}{2}\cos\left(\frac{(m-L_B+L_z+L_w)\pi}{L_w-1}\right) & \text{for } b_3 \le m < b_4 \\ 0 & \text{for } b_4 \le m < b_5\ , \end{cases} \tag{66}$$

where the boundaries b_i, for $i=1,\ldots,5$, are defined as $b_1=L_z$, $b_2=L_z+L_w$, $b_3=L_B-(L_w+L_z)$, $b_4=L_B-L_z$, and $b_5=L_B$, respectively. Now, the truncation can be implemented by weighting the generated sequence of burst samples with the respective window weights, that is

$$s_t[m]=w[m]s[m], \tag{67}$$

where $s_t[m]$ denotes the sample sequence of the truncated burst. The effective reduction in the length of the burst is controlled by L_z, the parameter defining the number of zero-weights (in the beginning and at the end) in the window $w[m]$, whereas the RC transitions are used to smoothen the sharp transients introduced by the cut-off operation. The sharpness of the RC-shaped transitions (i.e., the rapidity of the change of window coefficients from 0 to 1 (pre-tail) and from 1 to 0 (post-tail)) can be adjusted by controlling the value of L_w. The model of burst truncation based on a weighting window is illustrated in Figure 6-2.

6.3.1 Effect on symbol detection

Next, the effect of burst truncation on the detection performance of the effected symbols is analyzed. Assuming ideal channel, the estimate of the real-valued symbol, transmitted on the *k*th subcarrier during the *n*th symbol interval, can be expressed as

$$\tilde{d}_{k,n}=\mathrm{Re}\left\{\sum_{m=-\infty}^{\infty} s_t(m)e^{-j\frac{2\pi}{M}km}p(m-nM/2)\beta_{k,n}^{*}\theta_{k,n}^{*}\right\}. \tag{68}$$

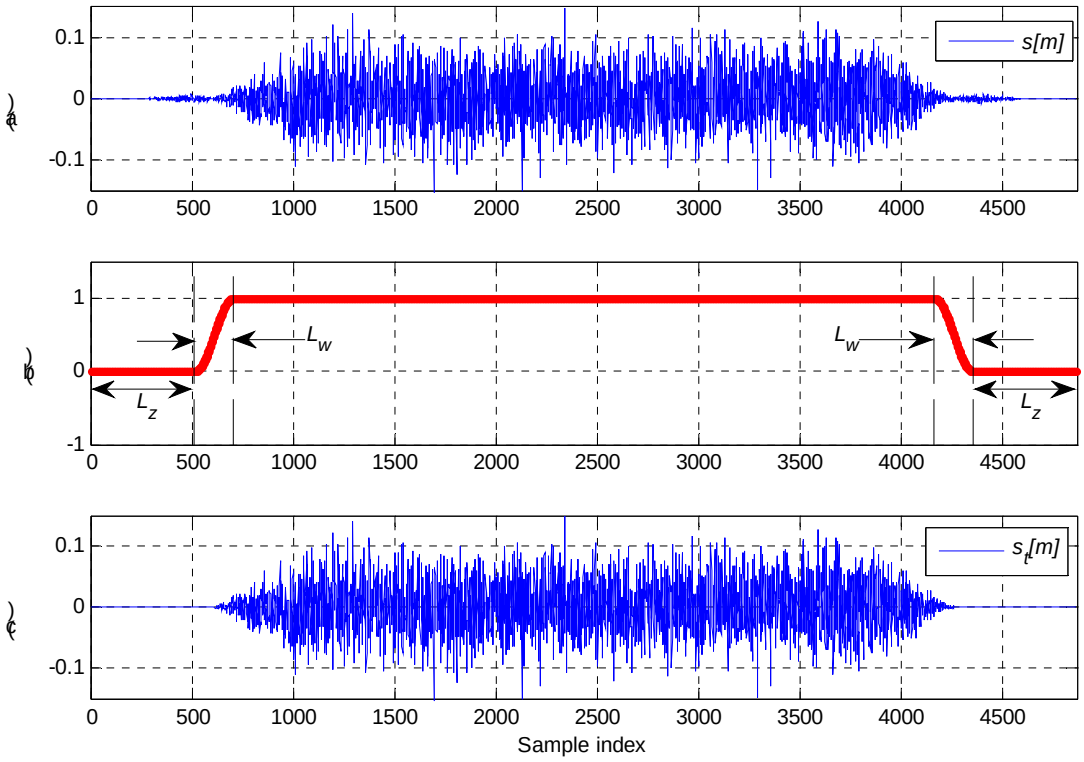

Figure 6-2. (a) Ideal burst $s[m]$, (b) weighting window $w[m]$, and (c) truncated burst $s_t[m]$.

Now, the normalized mean-squared error (MSE) at the OQAM sub-symbol detection (at rate $2/T$) can be expressed as

$$\Gamma(L_z, L_w, n) = E\left[\left(d_{k,n} - \tilde{d}_{k,n}\right)^2 / \sigma_d^2\right] = \frac{\sum_{b=1}^{N_b}\sum_{k=0}^{M}\left[\left(d_{k,n} - \tilde{d}_{k,n}(L_z, L_w)\right)^2 / \sigma_d^2\right]}{N_b M} \tag{69}$$

which is a function of the truncation window parameters L_z and L_w and the symbol index n. N_b denotes the number of bursts considered whereas $\sigma_d^2 = E\left[\left|d_{k,n}\right|^2\right]$ denotes the average symbol power. In a similar manner, the MSE at the OQAM symbol rate $1/T$ can be estimated based on the complex-valued symbols $c_{k,l}$ and $\tilde{c}_{k,l}$ (normalization by $\sigma_c^2 = E\left[\left|c_{k,l}\right|^2\right]$). Figure 6-3 shows the estimated MSE (in decibels) as a function of the effective truncation length L_z for the first six OQAM sub-symbols $(n = 0,1,\ldots,5)$ (left) and the corresponding OQAM symbols $(l = 0,1,2)$ (right) of the burst, respectively. Here, a weighting window with a RC-shaped transitions of $L_w = 33$ samples was used. The average MSE was estimated based on $N_b = 500$ burst truncations.

Clearly, more aggressive truncation results in an increased level of signal distortion and thus in higher MSE at detection. Moreover, following the intuition, the distortion gradually decreases with increasing symbol index n, indicating that the symbols located further away from the burst tails are

better protected. All the numerical results shown are based on the offset-QPSK (OQPSK) modulation.

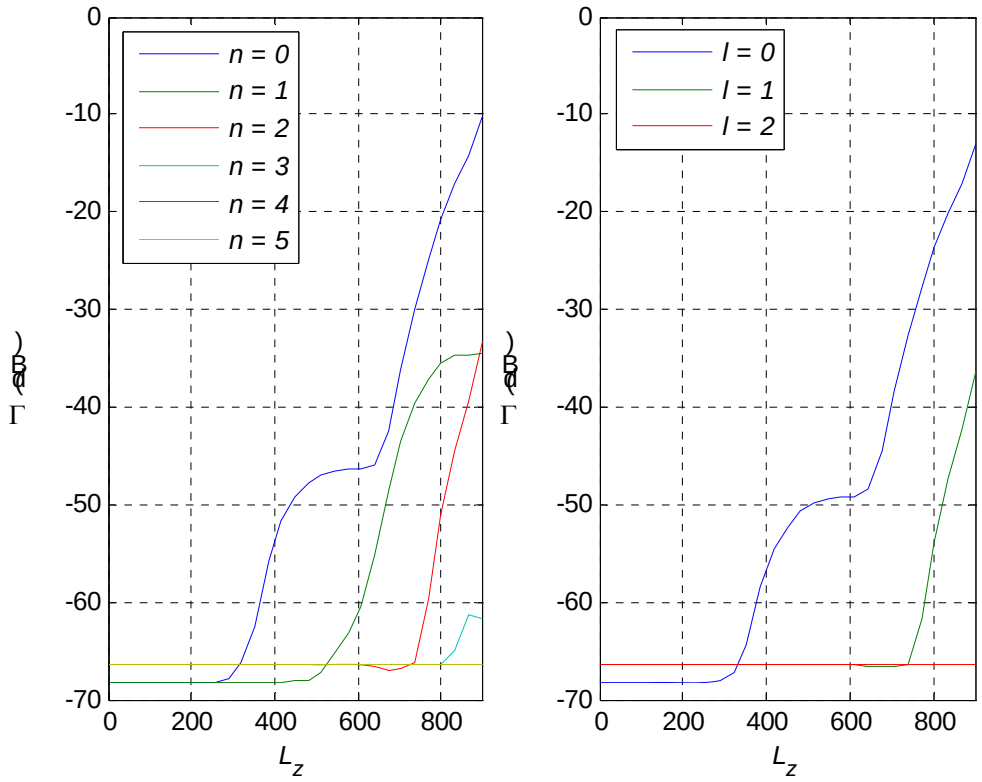

Figure 6-3. Effect of burst truncation on the detection performance of the burst tail symbols
$M = 512,\ K = 4,\ L_w = 33,\ L_z = [0:32:896],$ and $N_b = 500$.

6.3.2 Effect on spectrum

The burst truncation also influences the signal spectrum. To explore this effect we introduce a non-active part within the overall signal band by allocating zero-valued data to M_z subcarriers, that is $d_{k,n} = 0$ for subcarrier indexes from m_z to $m_z + M_z - 1$, where m_z denotes the reference index that defines the location of the non-active band. Now, the spectral regrowth due to burst shortening can be evaluated as

$$\Psi(L_z, L_w, n, k) = E\left[\left(d_{k,n} - \tilde{d}_{k,n}\right)^2 / \sigma_d^2\right] = \frac{\sum_{b=1}^{N_b}\left[\left(d_{k,n} - \tilde{d}_{k,n}(L_z, L_w, k)\right)^2 / \sigma_d^2\right]}{N_b}, \qquad (70)$$

for $k \in [m_z, m_z + M_z - 1]$, where the expectation is approximated by the sample average over $N_b = 500$ burst truncations. Figure 6-4 shows the estimated spectral leakage with different burst truncation lengths L_z as a function of subcarrier index k over the non-active part of the signal band, when a weighting window with RC -shaped transitions of $L_w = 33$ samples was used. More aggressive shortening results in more severe spectral regrowth outside the active signal band.

Moreover, similarly to MSE, also the degree of out-of-band leakage depends on the index of the investigated symbol in the burst. As observed in Figure 6-4 (right), during the fifth symbol interval ($n=4$) there is practically no leakage as the profile seen corresponds to the response of the prototype filter.

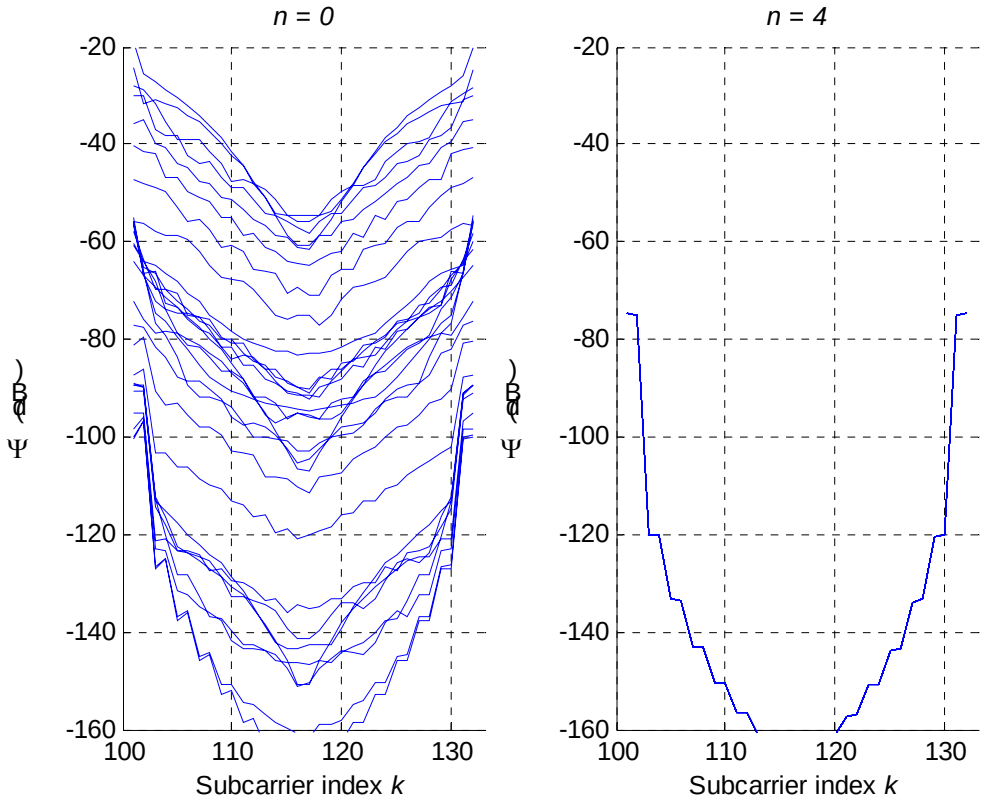

Figure 6-4. Effect of burst truncation on the out-of-band leakage during the first symbols of a burst. $L_w = 33,\ L_z = [0:32:896],\ N_b = 500,\ m_z = 101,\ M_z = 32,\ n = 0$ (left), and $n = 4$ (right).

6.4 Optimization of the truncation parameters

The MSE performance in symbol detection and the level of spectral leakage depend, in general, on both window parameters L_z and L_w. Therefore, it is necessary to evaluate both cost functions Γ and Ψ over a set of weighting window parameter combinations. Figure 6-5 shows the obtained MSE (left column) and leakage (right column) results for a variety of $\{L_z, L_w\}$ combinations. The top and the bottom row show the results for symbol index $n=0$ and $n=2$, respectively. Figure 6-5 indicates that the level of MSE depends dominantly on the choice of L_z. Furthermore, one can also observe a decaying MSE trend with decreasing number of RC-transition samples L_w. The out-of-band leakage is evaluated at the middle of the non-active band, i.e., for subcarrier index $k=116$. The level of spectral leakage depends strongly on the operation point $\{L_z, L_w, n, k\}$. It is dominantly influenced by the choice of L_z, while the effect of L_w depends strongly on the subcarrier index k considered in the evaluation. In general, however, a decaying leakage power trend with increasing number of RC-transition samples L_w can be observed. It should be noted that the severity of the distortion depends heavily on the observation time considered. The effects of truncating the burst tails decrease gradually with increasing symbol index n (i.e., for the symbols

within the body of the burst). This is clearly visible in the figures at the bottom row which show the results for the third ($n=2$) symbol of the burst, where a wide range of distortion-free $\{L_z\,;L_w\}$ values can be observed. Moreover, the criteria for selecting truncation parameters $\{L_z, L_w\}$ to minimize the MSE, on one hand, and the leakage, on the other, are partly contradicting.

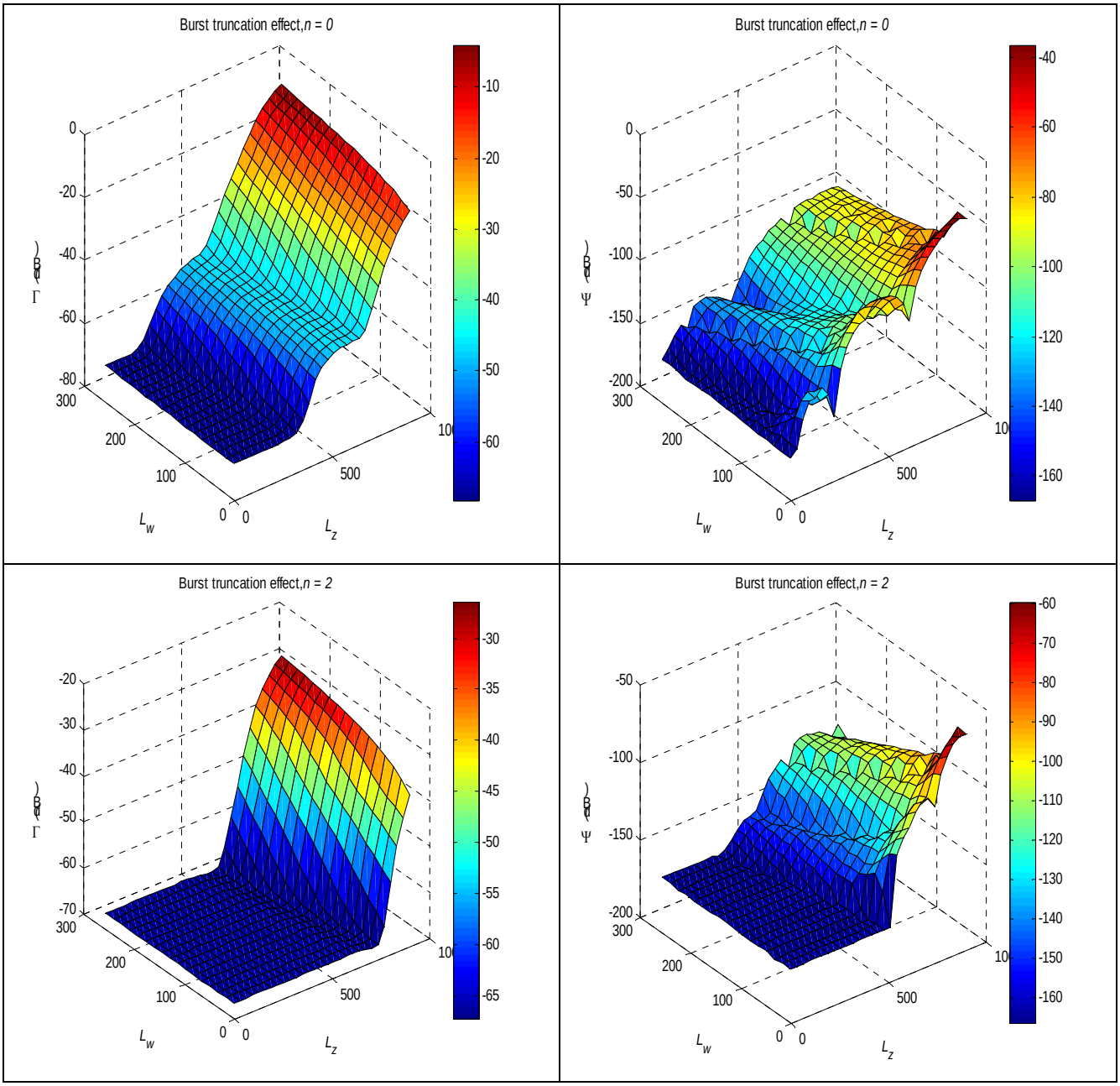

Figure 6-5. Mean-squared error $\Gamma(L_z, L_w)$ (left column) and out-of-band leakage $\Psi(L_z, L_w)$ (right column) during symbol interval $n=0$ (top row) and $n=2$ (bottom row), respectively.
$M=512$, $K=4$, $L_w=[1:16:257]$, $L_z=[0:32:896]$, $N_b=500$, $m_z=101$, $M_z=32$, and $k=116$.

A practical optimization problem of interest would be to search for such a combination of a maximum value of L_z, $L_{z,\text{opt}}$, and a minimum value of L_w, $L_{w,\text{opt}}$, that would simultaneously

maximize the spectral efficiency of the FBMC burst transmission and minimize the required processing, respectively. The optimization would be additionally constrained by the requirements that the choice of parameters have to fulfill the given MSE and leakage thresholds, T_Γ and T_Ψ, respectively, that is

$$\left\{L_{z,\mathrm{opt}}\,;L_{w,\mathrm{opt}}\right\}\left(T_\Gamma,T_\Psi\right)=\underset{\max L_z\,;\min L_w}{\arg}\left[\Gamma\left(L_z,L_w\right)\le T_\Gamma \quad \& \quad \Psi\left(L_z,L_w\right)\le T_\Psi\right]. \tag{71}$$

In order to evaluate the time domain overheads resulting from the optimized values of $L_{z,\mathrm{opt}}$ satisfying the given thresholds, T_Γ and T_Ψ, the number of required excess samples is defined according to

$$L_E = L_T - L_{z,\mathrm{opt}}\,. \tag{72}$$

Tables 6-1 and 6-2 show the results of optimization $\left\{L_E\,;L_{w,\mathrm{opt}}\right\}$, for a variety of threshold combinations $\left(T_\Gamma,T_\Psi\right)$, during the first symbol ($n=0$) when evaluated for the subcarrier index $k=102$ and $k=116$, respectively. Otherwise the simulation parameters are equivalent to those given in the previous section (see Figure 6-5 for clarification).

Table 6-1. Optimized burst truncation parameters for selected MSE and spectral leakage levels close to band edge. $\left\{L_{z,\mathrm{opt}}\,;L_{w,\mathrm{opt}}\right\}\left(T_\Gamma,T_\Psi\right)$ for $n=0,\ k=102$.

T_Γ (dB) / T_Ψ (dB)	-20	-30	-40	-50
-20	$\{96;1\}$	$\{160;1\}$	$\{224;1\}$	$\{448;1\}$
-30	$\{96;1\}$	$\{160;1\}$	$\{224;1\}$	$\{448;1\}$
-50	$\{192;1\}$	$\{192;1\}$	$\{224;1\}$	$\{448;1\}$
-70	$\{448;193\}$	$\{448;193\}$	$\{448;193\}$	$\{512;1\}$

Table 6-2. Optimized burst truncation parameters for selected MSE and spectral leakage levels at a distance of 16 subcarriers from band edge. $\left\{L_{z,\mathrm{opt}}\,;L_{w,\mathrm{opt}}\right\}\left(T_\Gamma,T_\Psi\right)$ for $n=0,\ k=116$.

T_Γ (dB) / T_Ψ (dB)	-20	-30	-40	-50
-40	$\{96;1\}$	$\{160;1\}$	$\{224;1\}$	$\{448;1\}$
-60	$\{128;33\}$	$\{192;17\}$	$\{224;1\}$	$\{448;1\}$
-80	$\{128;113\}$	$\{192;81\}$	$\{224;49\}$	$\{480;17\}$
-100	$\{192;193\}$	$\{320;33\}$	$\{320;33\}$	$\{480;49\}$

6.5 Impact on spectrum efficiency

In order to relate the obtained results to spectral efficiency evaluation of the FBMC transmission, a WiMAX framing example that takes into account the tails of FBMC bursts is considered. For the analysis, the following system parameters are assumed: channel bandwidth of 10 MHz, sampling frequency of 11.2 MHz, and FFT size of $M = 1024$. According to the WiMAX specifications, the OFDMA based reference system carries 47 OFDMA symbols within the 5 ms TDD frame. In case of FBMC, due to lack of cyclic prefixes, 54, 53, or 52 symbols could be transmitted within the 5 ms TDD frame, yet reserving 704, 1728, or 2752 samples for the FBMC burst tails, respectively. Assuming, that these intervals are evenly divided for the pre- and post-tails of the downlink and uplink subframes, each tail could be 176, 432, or 688 samples in length, respectively.

Figure 6-6 shows the mean-squared error (left column) and the out-of-band leakage (right column) for an FBMC burst with $\{176, 432, 688\}$ -sample pre- and post-tails, during the first ($n = 0$, top row) and the third symbol ($n = 2$, bottom row) interval, respectively. The results suggest that an FBMC frame structure consisting of 53 symbols could be a practical tradeoff between the spectral efficiency gain and the level of distortion due to burst tail truncation. This would mean that by utilizing FBMC modulation, six multicarrier symbols more could be transferred within a 5 ms WiMAX frame, compared to OFDM/QAM reference design. The spectral efficiency of FBMC modulation is further improved by exploiting the frequency selectivity of the subchannel spectrum to minimize the required frequency domain guard bands. Because of the good spectral containment of the prototype filter, a significantly higher number of active subcarriers can be considered in FBMC modulation based WiMAX transmission. In case of 10 MHz bandwidth, 913 active subcarriers (including the DC subcarrier) can be used for FBMC compared to the 841 subcarriers used in the OFDM reference design. Overall, these numbers correspond to a spectral efficiency gain of $\left(\frac{53\times 912}{47\times 840}-1\right)\times 100 \approx 22.4\%$ in the considered 5 ms WiMAX frame. When the neighbouring OFDMA multiplexes use FBMC waveforms, it is enough to have one subcarrier as the guard band, and the mentioned gain in spectrum efficiency can be achieved. However, when the adjacent multiplex is OFDM based, the usage of FBMC subcarriers around the band edge depends on the spectral mask specifications and assumed selectivity of the OFDM receivers.

It should be noted, however, that as the number of scheduled TDD uplink users within the uplink subframe is increased, the relative portion of the burst tails increases within the frame. This will reduce the spectral efficiency gain obtained with FBMC. Accurate estimation of the spectral efficiency, in such a case, requires a detailed analysis of the effects of placing the pre- and post-tails of consecutively scheduled uplink user bursts. In this case, burst truncation affects data symbols in a neighbouring subcarrier(s) during the tail transmission. On the other hand, the post- and pre-tails of different uplink users could potentially be scheduled to overlap in time. This is a research problem to be addressed in the continuation.

Moreover, it should be noted that in the uplink, an unused subcarrier is always required between different uplink users occupying neighbouring subcarrier blocks. This reduces the spectral efficiency of FBMC-based uplink transmission. This is especially a problem in the uplink PUSC mode.

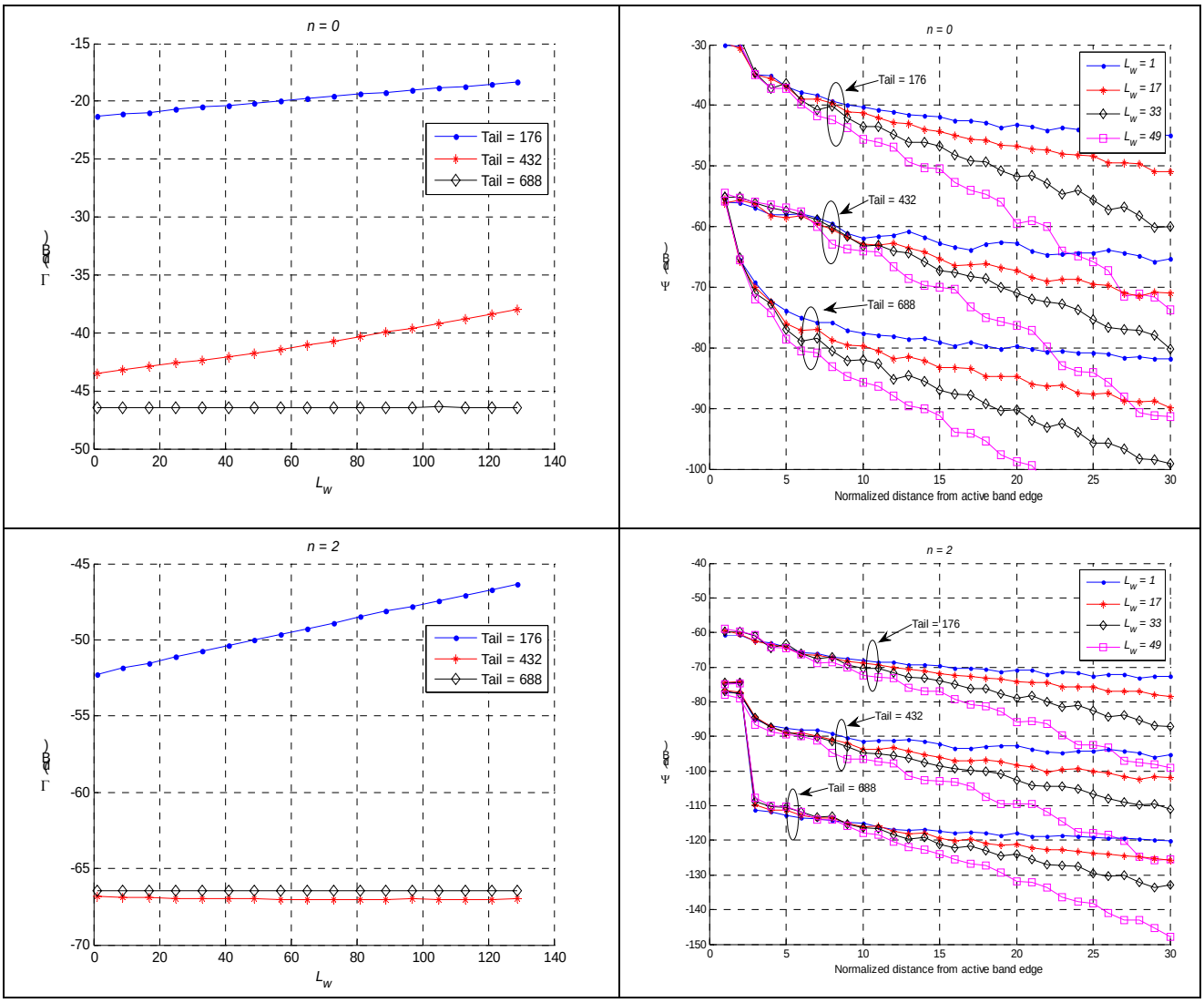

Figure 6-6. Mean-squared error (left column) and out-of-band leakage (right column) for an FBMC burst with $\{176, 432, 688\}$-sample pre- and post-tails during symbol interval $n = 0$ (top row) and $n = 2$ (bottom row), respectively: $M = 512$, $K = 4$, and $N_b = 500$.

7 Decision-directed timing synchronization in tracking

The objective of this section is to investigate one possible method for the tracking of the timing. This is obviously of great importance for the performance of the system, and has to be kept accurately during transmission. One first solution is to transfer the job of tracking the timing to the adaptive equalizer. As a matter of fact, the equalizer being able to adapt to changing conditions, can also adapt itself to the timing, to some extent, by changing its coefficients. This usually requires a multiple-tap equalizer. However, even with multiple tap equalizers, a complete tracking of the timing is impossible. If the timing goes off by more than 5-6% of the OQAM symbol, which corresponds to several samples, it is still needed to apply a correction and shift the position of the symbol at the receiver. In addition, in many situations, such as in the WiMAX environment, a single tap equalizer can be shown to be sufficient. This will also be shown in Deliverable 3.1 and is related to the typical channel characteristics and the design of the system, using high number of subcarriers. Hence, one remains with the options of using multiple-taps equalizers anyway in order to have increased timing capabilities, or to have a specific timing tracking algorithm.

In conclusion, it is clear that some tracking of the timing is necessary for the system, even if the required accuracy will depend on the type of equalizer used. Obviously, methods based on pilots, similar to the ones presented in section 4, can be used here. However, in order to limit the amount of pilots to be sent during the normal transmission of data, it is interesting to investigate other means of performing the timing adjustments, that require less or no pilots. Such a solution is proposed in this section. The main objective is to demonstrate that it is possible to obtain an acceptable synchronization performance with this kind of methods. It is based on a decision-directed algorithm and has a very low complexity. The algorithm is first described, and the performance is then evaluated theoretically.

7.1 Signal model

The system model is the same as described above. The OFDM/OQAM system has M subcarriers, some of them may remain unmodulated. The set of used subcarriers is denoted by M_u .The real and imaginary parts of the transmitted complex data symbols are separated in time by $T/2$ and transmitted in parallel on the different subchannels. The transmitted sequence, sampled at $T_s = T/M$ is given by

$$s(m) = \sum_{k \in M_u} \sum_{n=-\infty}^{\infty} d_{k,n} \theta_{k,n} g_k \left(m - nM/2 \right) \tag{73}$$

Note that all $d_{k,n}$ are here assumed real (they alternatively represent the real and imaginary parts of the complex data symbols). The coefficients $\theta_{k,l} = j^{k+l}$ account for the OQAM modulation alternating real and imaginary part. The transmitted sequence $s(m)$ feeds a DAC and propagates trough a physical channel characterized by impulse response $h(t)$ and AWGN noise $n(t)$. The received signal $r(t)$ is first filtered with an ideal low-pass filter of bandwidth $1/T_s$ and then sampled at frequency $f_s = 1/T_s$. The obtained sequence enters the analysis filter bank, and each output corresponding to each subcarrier, is filtered by its own equalizer $w_k(n)$ working at half of the

symbol time $T/2$. At the output of the equalizer, the real part or the imaginary part is taken depending on the symbol of interest and the subcarrier index.

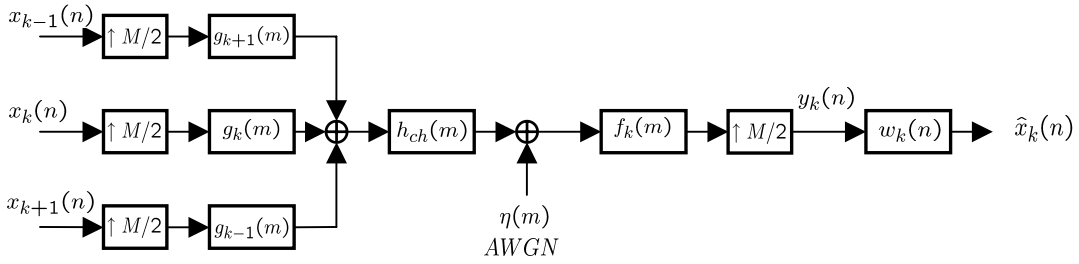

Figure 7-1: Block diagram of the transceiver

The cascade of all these effects can be written in the following way, assuming a one-tap equalizer for simplicity:

$$\tilde{d}_k(l) = \mathrm{Re}\left\{ \theta^*_{k,l} \sum_{k'=k-1}^{k+1} \sum_m d_{k'}(l-m)\theta_{k',l-m} x_{kk'}\left(m\frac{T}{2}+\tau \right) w_k(\tau) + \nu_k(l) \right\} \tag{74}$$

where $\tilde{d}_k(l)$ represents the symbol estimate at the output of the equalizer, $x_{kk'}(t)$ is the convolution of the synthesis filter for subcarrier k', the channel, the analysis filter for subcarrier k, w_k is the equalizer coefficient for the same subcarrier k; $\nu_k(l)$ is the additive noise component at the output of the equalizer, and τ is the timing error. We restrict ourselves to the single-user case. The multi-user case, for which the different users may have different timing errors τ_i, will be studied later. Note that the sum over k' is limited to neighbouring subcarriers only as the interference between distant subcarriers can be completely neglected.

The presence of $\theta^*_{k,l}$ ensures the correct OQAM demodulation. The equalizer coefficient is dependent on the timing. It is assumed here that the equalizer adaptation (necessary in a wireless channel) is faster than the timing jitter so that the equalizer constantly adapts itself to the new value of the timing. If a zero-forcing one-tap equalizer is used, this coefficient is just the inverse of the channel, or here the inverse of $x_{kk}(\tau)$, and the estimated symbol after equalization can be rewritten as

$$\tilde{d}_k(l) = \mathrm{Re}\left\{ \theta^*_{k,l} \sum_{k'=k-1}^{k+1} \sum_m d_{k'}(l-m)\theta_{k',l-m} x_{kk'}\left(m\frac{T}{2}+\tau \right) \frac{x^*_{kk}(\tau)}{\left|x_{kk}(\tau)\right|^2} + \nu_k(l) \right\}. \tag{75}$$

We will later use the following notation:

$$x_{kk',eq}\left(m\frac{T}{2}+\tau \right) = x_{kk'}\left(m\frac{T}{2}+\tau \right) \frac{x^*_{kk}(\tau)}{\left|x_{kk}(\tau)\right|^2}. \tag{76}$$

7.2 **Proposed Estimator**

The proposed estimator is based on the use of a TED (timing error detector) inside a closed loop, as represented in Figure 7-2. At each detected symbol, the TED provides a (noisy) estimate of the timing error (or proportional to the timing error). The estimated errors are filtered (and accumulated), and the actual timing is updated accordingly. In practice, for the considered system, only integer number of samples will be corrected, as it is not required to have a timing accuracy below the sampling time (the effect on the performance is negligible). Hence the loop will simply delay the OQAM symbol position by one sample in either direction when the accumulated estimation errors come above some threshold. Those kind of closed loop estimators are already well described in the literature [16]. The important block to design here is the TED.

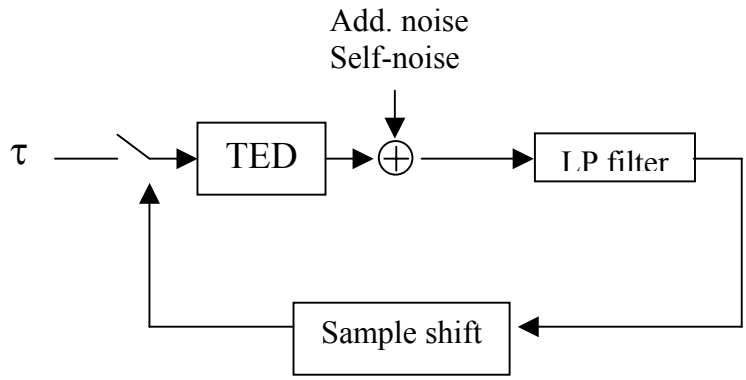

Figure 7-2: Closed loop timing synchonization

We propose a solution based on the well-known Mueller and Müller algorithm, adapted to the particular case of OQAM modulation. A similar development has been presented in [17] but for the case of real modulated filter banks only, and in a static environment where the equalizer is assumed to remain fixed. We generalize it here in order to be able to use it in the OQAM framework, and compute the performance in this particular case, for a wireless environment. The derivation is based on the ML principle, with many approximations in order to obtain a simple algorithm. The performance of the obtained algorithm will then be evaluated in order to check whether it is sufficient for the desired purpose despite the heavy approximations made in the derivation.

If we assume that the noise at the output of the equalizer is approximately white, and approximately independent between the different subcarriers, the likelihood of the set of equalizer outputs $\tilde{d}_k(n)$ for given input symbols $d_k(n)$ and for a fixed (unknown) value of the timing error τ can be written (up to a constant which is irrelevant) as

$$\Lambda\left(\tilde{d}\,|d,\tau\right) = -\sum_{k\in M_u}\sum_{l}\gamma_k\left|\tilde{d}_k(l) - \mathrm{Re}\left\{\theta^*_{k,l}\sum_{k'=k-1}^{k+1}\sum_{m} d_{k'}(l-m)\theta_{k',l-m}x_{kk',eq}\left(m\frac{T}{2}+\tau\right)\right\}\right|^2 \qquad (77)$$

The factors γ_k account for the fact that the noise variance is not necessarily the same on all carriers. It is assumed that the timing offset remains approximately constant at least for several consecutive symbols. Expanding (77), keeping only the double product which is the term containing most dependence on τ, and removing irrelevant constants, one obtains

$$\Lambda\left(\tilde{d}\,|d,\tau\right) \approx \sum_{k\in M_u}\sum_{l}\gamma_k \tilde{d}_k(l)\,\mathrm{Re}\left\{\theta^*_{k,l}\sum_{k'=k-1}^{k+1}\sum_{m} d_{k'}(l-m)\theta_{k',l-m}x_{kk',eq}\left(m\frac{T}{2}+\tau\right)\right\} \tag{78}$$

The timing error signal at time l is obtained by computing the derivative of this likelihood with respect to τ, taken at $\tau = 0$, and restricting ourselves to the contributions corresponding to equalizer outputs obtained at this instant l,

$$u_\Lambda(l) = \sum_{k\in M_u}\gamma_k \tilde{d}_k(l)\,\mathrm{Re}\left\{\theta^*_{k,l}\sum_{k'=k-1}^{k+1}\sum_{m} d_{k'}(l-m)\theta_{k',l-m}\dot{x}_{kk',eq}\left(m\frac{T}{2}\right)\right\} \tag{79}$$

where $\dot{x}_{kk',eq}(t)$ denotes the derivative of the impulse response $x_{kk',eq}(\Delta t+\tau)$ with respect to the timing offset. In order to have a simple algorithm, we further restrict the summation over time to 2 symbols, corresponding to $m=-2$ and $m=2$, and we neglect the cross-contributions for adjacent subcarriers, that is we assume that $x_{kk'}(t)$ for $k'\neq k$ can be neglected with respect to the direct contributions $x_{kk}(t)$:

$$u_\Lambda(l) = \sum_{k\in M_u}\gamma_k \sum_{m=-\{2,2\}} \tilde{d}_k(l)d_k(l-m)\,\mathrm{Re}\left\{\theta^*_{k,l}\theta_{k,l-m}\dot{x}_{kk,eq}\left(m\frac{T}{2}\right)\right\} \tag{80}$$

Of course, these equations are dependent on the particular realization of the channel. So we simplify the algorithm even further and assume that the impulse responses $x_{kk}(t)$ may be reasonably approximated by brickwall functions, of width corresponding to the subcarrier spacing. Now, the different values in the real part in (80) can be computed exactly and it is easily shown that it can be rewritten as

$$u_\Lambda(l) = \sum_{k\in M_u} K_k\left[\tilde{d}_k(l)d_k(l+2) - \tilde{d}_k(l)d_k(l-2)\right] \tag{81}$$

where the coefficients K_k need to be adjusted for the different subcarriers. So despite the complex nature of the OQAM transmitted signal, the obtained TED is very simple. It is very similar to the classical Mueller and Müller except it works with "real" and "imaginary" parts independently. It has a low complexity as it only requires 2 additional multiplications per subcarrier, which means it has a linear complexity in the number of subcarriers. No iterative search for a minimum is required as in many ML-based algorithms. Of course, many approximations have been made and it is now necessary to evaluate the performance of this algorithm in practice. Finally, in order to avoid any causality issue, we rearrange slightly the different terms of successive values of the TED outputs and write the final expression of the TED as

$$u_\tau(l) = \sum_{k\in M_u} K_k\left[\tilde{d}_k(l-2)d_k(l) - \tilde{d}_k(l)d_k(l-2)\right] \tag{82}$$

It is completely equivalent to the previous one since they are always included in a closed-loop, followed by an accumulator and a low-pass filter.

7.3 Performance analysis

The performance analysis is based on the usual tools for TED in closed-loop synchronization. We first evaluate the so-call S-curve of the TED, and then provide the PSD of the estimation error generated using this TED. The final performance, in terms of timing accuracy, depends on the choice of the filter used in the closed loop. It is outside of the scope of this deliverable to perform an analysis on this topic. We simply provide an example of results for a reasonable choice of the different parameters in the loop.

7.3.1 S-curve

The s-curve of the detector is the average value obtained for a fixed timing error τ. Using (81) and (75), performing the expectation, and using the following expressions based on the particular convention used for OQAM modulation, it is easily shown that the s-curve is given by

$$g(\tau) = \sum_{k \in M_u} K_k \sigma_{d_k}^2 \, \mathrm{Re}\left\{ x_{kk,eq}(-T+\tau) - x_{kk,eq}(T+\tau) \right\} \tag{83}$$

where $\sigma_{d_k}^2$ denotes the variance of the symbols $d_k(l)$.

Figure 7-3 shows one example of the S-curve obtained for a 1-tap equalizer, with 1024 subcarriers and a signal-to-noise ratio of $E_b / N_0 = 20\,\mathrm{dB}$. Even though it might not be optimal, we work with uniform weighting here ($K_k = 1$). The linearity of the detector is very good on the range of interest (about 10% of the symbol duration T). This kind of behaviour is observed in all cases, even when using it with a longer equalizer. The bias can also be shown to be very close to zero: $g(0) \approx 0$. It is in all cases orders of magnitude below the sample-level (T_s).

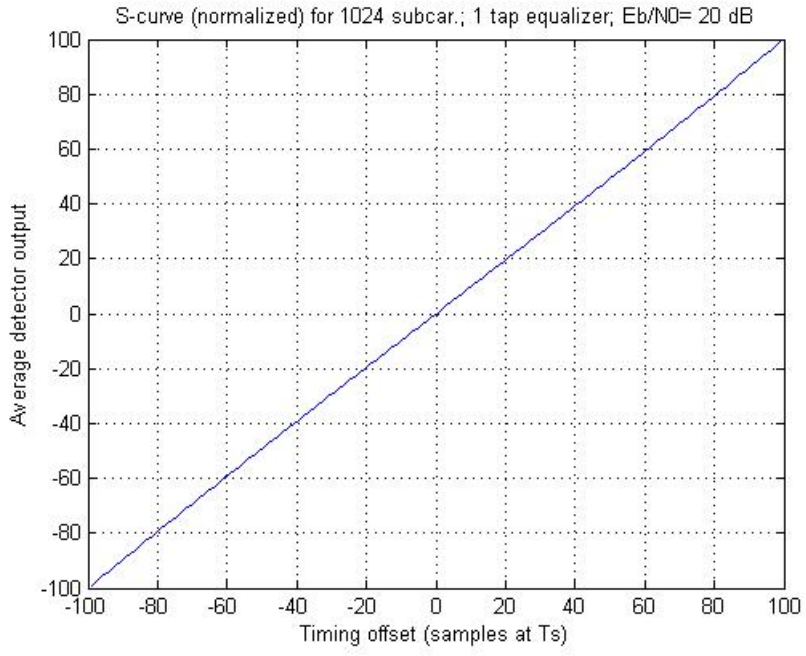

Figure 7-3: S-curve of the proposed timing error detector

7.3.2 Error variance

The analysis of the estimation error of the detector is done by computing the PSD of the total noise at the output of the detector. The total noise is the difference between the true value and the expected value (S-curve). It is usually split into an additive noise component, which depends only on the AWGN, and a self-noise component, which is related to the random nature of the data symbols $d_k(l)$. The TED output can be rewritten as

$$u_\tau(l) = g(\tau) + N_\nu(l) + N_s(l,\tau) \tag{84}$$

where $N_\nu(l)$ denotes the additive noise, the characteristics of which are independent of the timing error τ by stationary, and where $N_s(l,\tau)$ denotes the self-noise.

Based on (81) and (75), the contribution of the additive noise is

$$N_n(l) = \sum_k K_k \left[\mathrm{Re}\{\upsilon_k(l-2)\} d_k(l) - \mathrm{Re}\{\upsilon_k(l)\} d_k(l-2) \right] \tag{85}$$

The covariance $R_n(k)$ of the additive noise has only 3 components:

$$R_n(0) = 2\sum_k \sigma_{d_k}^2 K_k^2 \mathrm{E}\left[\mathrm{Re}\{\upsilon_k(l)\}^2 \right] \tag{86}$$

$$R_n(1) = R_n(-1) = \sum_k \sigma_{d_k}^2 K_k^2 \mathrm{E}\left[\mathrm{Re}\{\upsilon_k(l)\} \mathrm{Re}\{\upsilon_k(l-4)\} \right] \tag{87}$$

from which the PSD can easily be computed. Regarding the self-noise, its covariance depends on the value of the timing, so it is usually evaluated around the optimal timing $\tau = 0$. The full derivation is somewhat tedious, so we just state the final result:

$$\begin{aligned}
R_s(n) = \sum_{k,p} & K_k K_p \sigma_{d_k}^2 \sigma_{d_p}^2 \left[\mathrm{Re}\left\{ j^{k-p} j^{-n} x_{kp,eq}(nT/2 - T) \right\} \mathrm{Re}\left\{ j^{p-k} j^{n} x_{pk,eq}(-nT/2 - T) \right\} \right. \\
& -2\,\mathrm{Re}\left\{ j^{k-p} j^{-n} x_{kp,eq}(nT/2) \right\} \mathrm{Re}\left\{ j^{p-k} j^{n} x_{pk,eq}(-nT/2) \right\} \\
& \left. +\,\mathrm{Re}\left\{ j^{k-p} j^{-n} x_{kp,eq}(nT/2 + T) \right\} \mathrm{Re}\left\{ j^{p-k} j^{n} x_{pk,eq}(-nT/2 + T) \right\} \right] \\
& +2\delta_n \sum_{k,p} K_k^2 \sigma_{d_k}^2 \sigma_{d_p}^2 \sum_m \mathrm{Re}\left\{ j^{k-p} j^{-m} x_{kp,eq}(mT/2) \right\}^2 \\
& -\delta_{n+2} \sum_{k,p} K_k^2 \sigma_{d_k}^2 \sigma_{d_p}^2 \sum_m \mathrm{Re}\left\{ j^{k-p} j^{-m} x_{kp,eq}(mT/2) \right\} \mathrm{Re}\left\{ j^{k-p} j^{-m} x_{kp,eq}(mT/2 + 2T) \right\} \\
& -\delta_{n-2} \sum_{k,p} K_k^2 \sigma_{d_k}^2 \sigma_{d_p}^2 \sum_m \mathrm{Re}\left\{ j^{k-p} j^{-m} x_{kp,eq}(mT/2) \right\} \mathrm{Re}\left\{ j^{k-p} j^{-m} x_{kp,eq}(mT/2 - 2T) \right\} \\
& +\delta_n \sum_k K_k^2 \left[\sigma_{d_k}^4 - 3\left(\sigma_{d_k}^2\right)^2 \right] \left[\mathrm{Re}\left\{ x_{kk,eq}(-T) \right\}^2 + \mathrm{Re}\left\{ x_{kk,eq}(T) \right\}^2 \right] \\
& -\delta_{n+2} \sum_k K_k^2 \left[\sigma_{d_k}^4 - 3\left(\sigma_{d_k}^2\right)^2 \right] \mathrm{Re}\left\{ x_{kk,eq}(-T) \right\} \mathrm{Re}\left\{ x_{kk,eq}(T) \right\} \\
& -\delta_{n-2} \sum_k K_k^2 \left[\sigma_{d_k}^4 - 3\left(\sigma_{d_k}^2\right)^2 \right] \mathrm{Re}\left\{ x_{kk,eq}(-T) \right\} \mathrm{Re}\left\{ x_{kk,eq}(T) \right\}
\end{aligned} \tag{88}$$

The important observation here is that all the terms in (88) are based on values of $x_{kp,eq}(t)$ which are very small, by design of the OQAM system. For instance, it is easy to show that all the terms of the form

$$\mathrm{Re}\left\{ j^{k-p} j^{-m} x_{kp,eq}(mT/2) \right\} = \mathrm{Re}\left\{ \theta_{k,l}^* \theta_{p,l-m} x_{kp,eq}(mT/2) \right\} \tag{89}$$

are very close to zero since they correspond to the interference between the transmitted symbols. Consequently, the self-noise will be low. Figure 7-4 shows the PSD of the additive noise and self-noise computed from these expressions, again in the uniform weighting case ($K_k = 1$ for all k) which is not optimal.

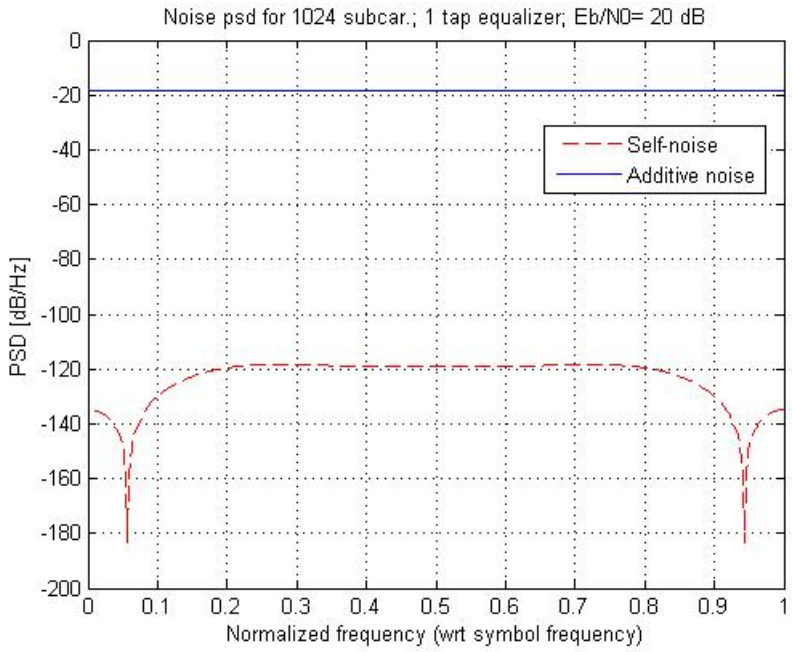

Figure 7-4: Noise PSD of the TED

In practice, only the low frequency part of the PSD does matter as the higher frequency part will be filtered by the filter in the closed loop. It can be seen that the self-noise is very low. The additive noise is almost white (flat). With the results obtained here, and assuming a loop bandwidth around 50 Hz (based on typical specifications of sampling clock precision), the timing jitter variance obtained with this method is around $\sigma_\tau^2 = 1.25\ 10^{-4}$, normalized with respect to the symbol duration. It means that the system remains with a timing jitter with a standard deviation of around 1% of the symbol duration, which is perfectly acceptable.

The proposed TED could be further optimized on the weighting factors K_k in order to improve the performance further. In particular, it should take into account the different SNR's obtained at the different subcarriers depending on the channel (which is adaptively estimated). This optimization is left for further work. Finally, the influence of the decision errors also needs to be investigated. At a typical BER of 10^{-3}, this effect is very limited however, and the algorithm is somewhat protected from error propagation thanks to the adaptation of the equalizer (a limited amount of error is always corrected by the equalizer).

In conclusion, this section has shown that it is a viable solution to perform the tracking of the timing error without the help of pilots. The proposed solution also has a limited complexity.

8 Conclusion: Synthesis of work done, achievements, issues and future work

This report deals with the problem of data-aided synchronization and initialization for FBMC systems. Precisely, after a brief presentation of the FBMC system and a description of the signal model, it has been analyzed the problem of synchronization and initialization for FBMC systems in two different situations, namely for the full block of sub-channels and for a group of sub-channels. For the full block of sub-channels, the situation is the same as for OFDM. Existing standards for OFDM systems (e.g., WiFi or WiMAX) exploit training sequences for optimal carrier frequency offset and timing estimation. The case of groups of sub-channels is specific to FBMC, due to the independence of sub-channels in the scheme. A key aspect is that a significant part of the operations have to take place after the filter bank in the receiver.
In chapter 4 preamble-based synchronization algorithms for symbol timing, carrier phase and CFO estimation for uplink and downlink of an OFDM/OQAM system have been considered. Specifically, in section 4.1 a synchronization scheme based on a training sequence made up of identical parts has been considered. The proposed method is based on the LS approach, it operates in the time domain before running the receiver filter bank, and, moreover, it does not require the knowledge of the channel impulse response and of the SNR. The performance of the derived LS estimator has been assessed via computer simulation and compared with that of a modified version of two previously proposed joint symbol timing and CFO estimators. Specifically, numerical results have shown that the proposed estimators assure a particular robustness in the presence of a multipath channel providing estimates whose accuracy is quite similar to that achieved in AWGN.

Section 4.2 (Section 4.3) deals with the problem of data-aided symbol timing (CFO) synchronization in the uplink of a multiuser OFDM/OQAM system. In particular, we have derived the joint ML estimator for the phase offset and the symbol timing (the joint ML estimator for the CFO and the phase offset) of each of U users, and we have shown that this approach leads to U different joint phase offset and symbol timing (phase offset and CFO) estimators. Moreover, since for each user the phase estimate is in closed form, the symbol timing (CFO) estimator requires only a one-dimensional maximization procedure with respect to a continuous parameter. The performance of the proposed ML estimator has been assessed via computer simulations both in AWGN and multipath channel, and for three different allocation schemes. The numerical results have shown that the ML estimator can assure accurate estimates with only two training symbols if the total number of subcarriers is sufficiently large

Future work in this context includes studies on simplified estimation algorithms in the uplink of a multiuser OFDM/OQAM system that could assure satisfactory performance at a low computational cost. It is also important to analyze the applicability of the considered estimation algorithms in a typical WiMAX configuration for Lab performance comparisons expected in WP9. Further, in some situations, particularly for small groups of sub-channels or a single sub-channel, the use of training sequences can involve a significant overhead, leading to a spectral efficiency reduction, thus non data-aided (or blind) techniques will be studies and contrasted with data-aided schemes.

Regarding pilot based CFO estimation and symbol timing, in chapter 6 it has been studied the performance of a pilot scheme proposed in literature [13] that is able to adapt the WiMAX pilot configurations to be used with FBMC. The investigated auxiliary pilot approach is based on the elimination of the interference on the complementary (imaginary/real) part of the (real/imaginary) pilots in case of ideal channel transmission. Initial evaluation has returned adequate dimensioning

parameters for this scheme within WiMAX pilot scattering modes and the filter bank prototype currently considered.

The application of the auxiliary pilot scheme to channel estimation is straight-forward, and it also allows for simple CFO and symbol timing estimation methods. In case of CFO, pilots within a subcarrier experience a phase rotation with time proportional to the CFO. Using the studied pilot scheme, this phase rotation can be directly measured and averaged over different subdivisions of the transmitted burst to return a robust (within most of the range of unambiguity) and accurate estimate (RMS error < 0.1% of subcarrier spacing) of the CFO even at bad channel conditions. The unambiguity range is defined by the pilot separation in time. In the WiMAX AMC-23 mode the range is 1/6 of the subcarrier spacing, in DL-PUSC it can be reduced to 1/3 of the spacing, with correct pilot selection. That is, ±1.82 kHz and ±3.65 kHz, respectively.

In principle, it is possible to use an analogous method to assess the phase rotation with respect to the frequency to obtain fractional timing delay (FTD) estimates. Evaluation has shown that the performance in practical channel conditions is much worse than for CFO, though. Therefore, we have developed a method that jointly estimates the channel and the symbol timing in an iterative fashion. Preliminary results return a maximum RMS estimation error of around 2% (22 samples with the 1k WiMAX dimensioning) for delays of up to 50% of the OQAM symbol interval. However, this method is more sensitive to the number of pilots used to perform the estimation than the CFO estimation technique presented above.

Immediate efforts are dedicated to evaluate the joint timing and channel estimation method more thoroughly and with different pilot configurations and channel conditions. As a matter of fact, the auxiliary pilot based channel estimation method appears very sensitive to FTD, therefore, a great advantage is hoped for when applying the joint estimation method.

In the longer term, we plan to include in these studies alternative approaches to obtain pilot based estimates [14] and compare their performances and complexities with the presented method. Once the limitations of these techniques are fully understood, we will study, in conjunction with WP3, if a pilot scattering different from the standardized by WiMAX can be proposed to reduce the overhead of an alternative PHYDYAS scheme. Another possible advantage example is widening the unambiguity range by placing two pilots as consecutive symbols.

The overlapping nature of the base functions in filter banks implies that there are certain tails containing signal energy before and after the actual data transmission. Since this can pose a threat to the good expected spectral efficiency, we have researched the effect of reducing the length of these tails by adequate truncation and windowing. The shortening of the tails introduces distortion on the symbols closest to the beginning and the end of the transmitted burst. Further, the burst shows a spectral regrowth at adjacent frequencies during the beginning and the end of the burst. We have evaluated the MSE due to the distortion and the spectral regrowth. Based on this, we have optimized the length and windowing of the remaining tails to keep the undesired effects under an acceptable limit. With the optimized values we have dimensioned an alternative FBMC burst for the 10 MHz / 5 ms WiMAX specifications in which we gain around 22.4% in spectral efficiency. This is because we can use a few more symbols in time domain and quite a lot more carriers for data transmission.

Future work in this context includes studies of the effect of the burst truncation and the acceptable amount of overlap between user-bursts in a TDD multiuser (uplink) scenario. It is also important to

measure the effect on data-aided synchronization and channel estimation, since this is a further source of distortion. This is especially grave when using a preamble generated and then processed in frequency domain, since that preamble is most affected by the truncation. In this sense, joint optimization of the burst truncation, filter bank preloading and preamble design is a subject of future research.

REFERENCES

[1] P. Siohan, C. Siclet and N. Lacaille, "Analysis and design of OFDM/OQAM systems based on filterbank theory," *IEEE Trans. Signal Processing*, pp 1170-1183, May 2002.

[2] M.G. Bellanger, "Specification and design of a prototype filter for filter bank based multicarrier transmission," in *Proc. Int. Conf. Acoustics, Speech, and Signal Processing* (ICASSP '01), pp. 2417 – 2420, May 2001.

[3] H. S. Malvar, *Signal Processing with Lapped Transforms*, Artech House, Norwood, Mass, USA, 1992.

[4] P.P. Vaidyanathan, *Multirate Systems and Filter Banks,* Prentice Hall, Englewood Cliffs, NJ, USA, 1993

[5] T. Ihalainen, T. Hidalgo Stitz, M. Rinne, and M. Renfors, "Channel equalization in filter bank based multicarrier modulation for wireless communications," EURASIP Journal on Advances in Signal Processing, vol. 2007, pp. Article ID 49 389, 18 pages, 2007, doi:10.1155/2007/49389.

[6] T. Karp, N.J. Fliege, "Modified DFT filter banks with perfect reconstruction," *IEEE Trans. Circuits and Systems II*, vol. 46, pp. 1404-1414, Nov. 1999.

[7] Deliverable 3.1, "Transmit/receive processing (single antenna)," ICT-211887 PHYDYAS, July 2008.

[8] T. H. Stitz, T. Ihalainen, M. Renfors, "Practical issues in frequency domain synchronization for filter bank based multicarrier transmission," *Proc. of Third International Symposium on Communications, Control and Signal Processing*, S. Julians, Malta, 12-14, Marzo, 2008.

[9] T. Fusco, A. Petrella and M. Tanda, "Data-aided time-domain synchronization for filter bank multicarrier systems," in *Proc. 16th European Signal Processing Conference*, Lausanne 24-29 August 2008.

[10] A. Tonello and F. Rossi, "Synchronization and Channel Estimation for Filtered Multitone Modulation, " *in Proc. of WPMC 2004*, Abano Terme, pp. 590-594, Sept. 2004.

[11] T. Fusco, A. Petrella and M. Tanda, "Data-aided symbol timing and CFO synchronization for filter bank multicarrier systems," submitted to *IEEE Trans. Wireless Communications.*

[12] T. Schmidl, D. Cox, "Robust Frequency and Timing Synchronization for OFDM," *IEEE Trans. Comm*., pp. 1613-1621, December 1997.

[13] J.-P. Javaudin, D. Lacroix, A. Rouxel, "Pilot-aided channel estimation for OFDM/OQAM," in *Proc. Vehicular Technology Conf. (VTC 2003-Spring),* pp. 1581-1585, April 2003.

[14] C. Lele, J.-P. Javaudin, R. Legouable, A. Skrzypczak, P. Siohan, "Channel estimation methods for preamble-based OFDM/OQAM modulations," in *Proc. European Wireless 2007*, Paris, France, April 2007.

[15] M. Morelli, C.-C. Kuo, M.-O. Pun, "Synchronization Techniques for Orthogonal Frequency Division Multiple Access (OFDMA): A Tutorial Review," Proc. IEEE, vol. 95, pp. 1394-1427, July 2007.

[16] H. Meyr, M. Moeneclaey, S. Fechtel, "Digital Communications", Wiley Interscience, 1993.

[17] J. Louveaux, L. Cuvelier, L. Vandendorpe, and T. Pollet, "Baud rate timing recovery scheme for filter-bank based multicarrier transmission", *IEEE Trans. on Commun.*, vol. 51, No. 4, April 2003, pp. 652-663.